Journal of Hazardous Materials Advances 20 (2025) 100905

Contents lists available at ScienceDirect

Journal of Hazardous Materials Advances

journal homepage: www.elsevier.com/locate/hazadv

Developing environmentally relevant test materials for microplastic research through UV-induced photoaging

Serena Ducoli [a,†], Claudio Marchesi [a,†], Mario Rigo [a], Annalisa Zacco [a], Erika Caianiello [b], Rachele Castaldo [b], Mariacristina Cocca [b], Stefania Federici [a,*], Laura Eleonora Depero [a]

[a] Chemistry for Technologies Laboratory, Department of Mechanical and Industrial Engineering, University of Brescia & INSTM RU of Brescia, via Branze, 38, 25123 Brescia BS, Italy

[b] Institute of Polymers composites and Biomaterials National Research Council of Italy, Via Campi Flegrei, 34, 80078 Pozzuoli NA, Italy

ARTICLE INFO

Keywords:
True-to-life microplastics
Photodegradation
Carbonyl index
Test materials
Environmental relevance

ABSTRACT

Microplastics (MPs), defined as plastic fragments smaller than 1 mm, are pervasive pollutants posing considerable ecological and health hazards owing to their durability and potential to cause adverse environmental effects. These particles originate mainly from the breakdown of bigger plastic debris by mechanisms such as UV-induced photodegradation, resulting in fragmentation into micro- and nanoplastics. Appropriate laboratory test materials that simulate naturally degraded plastics are essential for evaluating the environmental impact of MPs, enhancing analytical methods, and assessing remediation pathways. In this study we generated "true-to-life" MPs from commonly utilized plastic products through controlled photodegradation processes designed to accelerate polymer aging. Two aging protocols were developed: (i) UV irradiation of macroplastic fragments for up to eight weeks followed by mechanical milling, and (ii) UV exposure of pre-fragmented MPs over the same period. Five polymers, namely polystyrene (PS), polypropylene (PP), high-density polyethylene (HDPE), polyvinyl chloride (PVC), and polyethylene terephthalate (PET), were chosen for analysis, with PET investigated separately due to the presence of the carbonyl group, which complicates carbonyl index (CI) calculations used as a quantitative index to monitor the photo-oxidation. The surface morphology of aged MPs was examined using Scanning Electron Microscopy (SEM), their chemical composition was investigated by Near-Infrared (NIR) and Fourier-transform Infrared (FTIR) spectroscopy, thermal properties were also evaluated by Thermogravimetric Analysis (TGA). PET degradation was further analyzed using supplementary techniques such as X-Ray Diffraction (XRD) and Differential Scanning Calorimetry (DSC) to assess structural and thermal alterations. These findings demonstrate that the proposed protocols generate MPs with consistent physicochemical properties, providing a model system suitable for studying MP degradation and behavior in laboratory studies, ultimately supporting environmental risk assessment and mitigation strategies.

1. Introduction

Microplastics (MPs) are defined as “any solid plastic particle insoluble in water with any dimension between 1 μm and 1 000 μm”, according to the ISO standard definition, while a broader and more widely used definition also includes plastic fragments smaller than 5 mm, with ‘large microplastics’ referring to those between 1 mm and 5 mm (ISO/TR 21960: 2020 2020). MPs have become pervasive in various ecosystems, raising serious environmental and health concerns due to their persistence and potential for harm (De Boever et al., 2024). Some of these particles are derived from the degradation of larger plastic items, resulting from physical, chemical, and biological processes, such as mechanical abrasion, photodegradation, and chemical weathering (S. Kumari et al., 2025). Among these, photodegradation due to UV exposure is one of the most significant pathways, as plastics in natural environments are often exposed to sunlight for extended periods (Singh et al., 2025; Zhang et al., 2025). This results in changes in both their morphology and chemical composition, eventually leading to fragmentation and the formation of micro- and nanoplastics.

Due to the pervasive occurrence and potential hazards associated

* Corresponding author.
E-mail address: stefania.federici@unibs.it (S. Federici).
† co-first authorship.

https://doi.org/10.1016/j.hazadv.2025.100905
Received 30 June 2025; Received in revised form 15 September 2025; Accepted 29 September 2025
Available online 1 October 2025

with MPs, it is imperative to create reliable laboratory test materials that can replicate the weathered plastics present in the environment (Ducoli et al., 2025). These materials not only simulate the physicochemical modifications that plastics experience in real-world environments but are also essential for understanding the behavior, persistence, and interactions of MPs with other elements in both aquatic and terrestrial ecosystems. The ecological significance of these test materials guarantees that laboratory findings may be more precisely extrapolated to natural environments, allowing researchers to more effectively assess the possible effects of MPs on ecosystems and human health. Furthermore, the creation of reliable test materials that closely mimic naturally degraded plastics is essential for enhancing analytical methods for MP identification and quantification, as well as for evaluating the efficacy of remediation solutions in realistic scenarios.

In recent decades, increasing attention has been devoted to understanding the effects of UV irradiation on plastic degradation in natural environments (Hernandez et al., 2025; S. Kumari et al., 2025). These studies primarily aimed to elucidate the mechanisms of degradation, the fragmentation dynamics, and the physicochemical surface changes plastic undergo under environmental conditions, especially in the marine environment (E. Kuka et al., 2024; Strohriegl et al., 2021). Increases of carbonyl index (CI) and crystallinity, mass loss, and the formation of surface fractures have been observed in polypropylene and polyethylene terephthalate packaging materials subjected to dry-air UV irradiation (W. Conradie et al., 2022). Accelerated photooxidation experiments demonstrated the generation of micro- and nanoplastics from virgin and additive-containing polypropylene under simulated sunlight exposure (Song et al., 2023), while irradiation of environmental fragments of polyethylene and polystyrene produced abundant particles smaller than 2 μm, including nanoplastics in the sub-micron range (Sorasan et al., 2022).

However, only a limited number of studies have investigated how the modifications induced by photo-degradation, such as the formation of new functional groups, the release of degradation by-products, or changes in particle size, morphology, and surface chemistry, affect MP role in transport, adsorption, and eco-toxicity processes (Wang et al., 2025). This gap is largely due to the lack of environmentally relevant test MPs and the absence of standards or guidelines for their production. Available ISO/ASTM standards focus on protocols for exposing plastics to laboratory light sources under controlled environmental conditions, but there are no standard methods intended for driving the production of reference aged MPs.

In this context, the aim of our work is to propose a robust protocol for generating environmentally relevant “true-to-life” MPs, by integrating controlled mechanical fragmentation with UV-induced degradation. By true-to-life approach, we refer to secondary MPs generated at the laboratory scale through mechanical fragmentation techniques from everyday plastic products, closely resembling those found in natural environments in terms of size, morphology, and chemical composition. These starting products, which retain the original composition imparted during manufacturing — including polymers, additives, and other formulation components — introduce variability that significantly increases the environmental relevance of the test materials. This, in turn, allows for a more accurate reflection of the diversity of plastics found in the environment and the complex ways they degrade over time (S. Ducoli et al., 2024; S. Ducoli et al., 2024). We developed and compared two UV-aging protocols applied to mechanically fragmented MPs from five widely used polymers: polystyrene (PS), polypropylene (PP), high-density polyethylene (HDPE), polyvinyl chloride (PVC), and polyethylene terephthalate (PET). The generated test materials were systematically characterized through Near-Infrared (NIR) spectroscopy, Fourier-transform Infrared (FTIR) spectroscopy, Thermogravimetric Analysis (TGA), and Scanning Electron Microscopy (SEM), while for polyethylene terephthalate (PET) samples additional insights were obtained by X-Ray Diffraction (XRD) and Differential Scanning Calorimetry (DSC). Such an approach is intended to provide reproducible and realistic test microparticles to support future research on the environmental behavior and impacts of micro- and nanoplastics, and to lay the foundation for the harmonization of laboratory tests and protocols for the production and aging of environmentally relevant test MPs.

2. Materials and methods

2.1. Experimental plan

We investigated the artificial photodegradation of true-to-life MP particles through two distinct aging protocols, each designed to mimic different environmental scenarios (Fig. 1). In the first protocol, macroplastic pieces were subjected to UV irradiation for up to eight weeks, with pieces removed weekly and fragmented through cryogenic mechanical milling. In the second protocol, plastic fragments were initially fragmented through cryogenic milling, and these MPs were then aged under UV exposure for the same period (see representative pictures of the experimental setup in Figure S1 in the Supplementary Material). Chemical composition of MP fragments was investigated by NIR, coupled with chemometric analysis, and FTIR spectroscopy. To evaluate the degradation level, theCI was calculated based on FTIR spectra and compared for the two different approaches. Surface morphologies of MP fragments selected from the second aging protocol were characterized by means of SEM. TGA was also performed in order to better understand how the selected aging protocol affected the thermal properties of the materials. Five polymers, namely PS, PP, HDPE, PVC, and PET were selected. The case of PET was treated separately, as the presence of the carbonyl group due to the ester bond made the calculation of the CI very challenging, since the carbonyl is already strongly present in the unaged molecule. To better understand PET degradation behavior, complementary analyses including XRD and DSC were incorporated. These techniques provided additional insights into possible PET structural and thermal changes during photoaging.

2.2. Materials

Five types of plastic materials sourced from everyday plastic products were selected for this study: PS, PP, HDPE, PVC, and PET. In the first protocol (Fig. 1a), all samples were initially cut into approximately 8 cm pieces using stainless steel scissors, then immersed in a bath containing Milli-Q (Millipore Co., Bedford, USA, MA) water and detergent to remove dirt and grease. After thorough washing with Milli-Q water, the samples were dried. During the eight-week UV aging process, pieces of each polymer were removed from the UV box weekly. These pieces were cryogenically pre-treated by immersion in liquid nitrogen for 30 min to embrittle the material and prevent thermal degradation during the subsequent mechanical fragmentation. The samples were then fragmented using a mixer mill (MM400, Retsch GmbH, Haan, Germany) for 10 min at a frequency of 30 Hz, with 9 stainless steel spheres (10 mm diameter) in 35 ml jars previously cooled down in liquid nitrogen. After milling, the samples were sieved to ensure that the resulting MPs had a maximum particle size of 500 μm in at least one dimension before being stored for subsequent characterization. Further details on the mechanical fragmentation protocol and the resulting MP properties (morphology, size distribution, crystallinity) are available in our previous studies (Ducoli et al., 2025; Marchesi et al., 2023).

In the second protocol (Fig. 1b), plastics of the same polymeric composition were selected from different plastic objects to increase the heterogeneity of the test materials, both in terms of manufacturing and, possibly, the additives content. As with the first protocol, all samples were cleaned by immersion in a Milli-Q water and detergent bath, followed by rinsing and drying. The samples were then manually cut into small pieces, approximately 0.5 cm in size, and cryogenically milled before the aging process, using the same steps as the first protocol. The MPs were then subjected to UV exposure for the duration of the study.

For each type of plastic and both protocols, unaged samples were

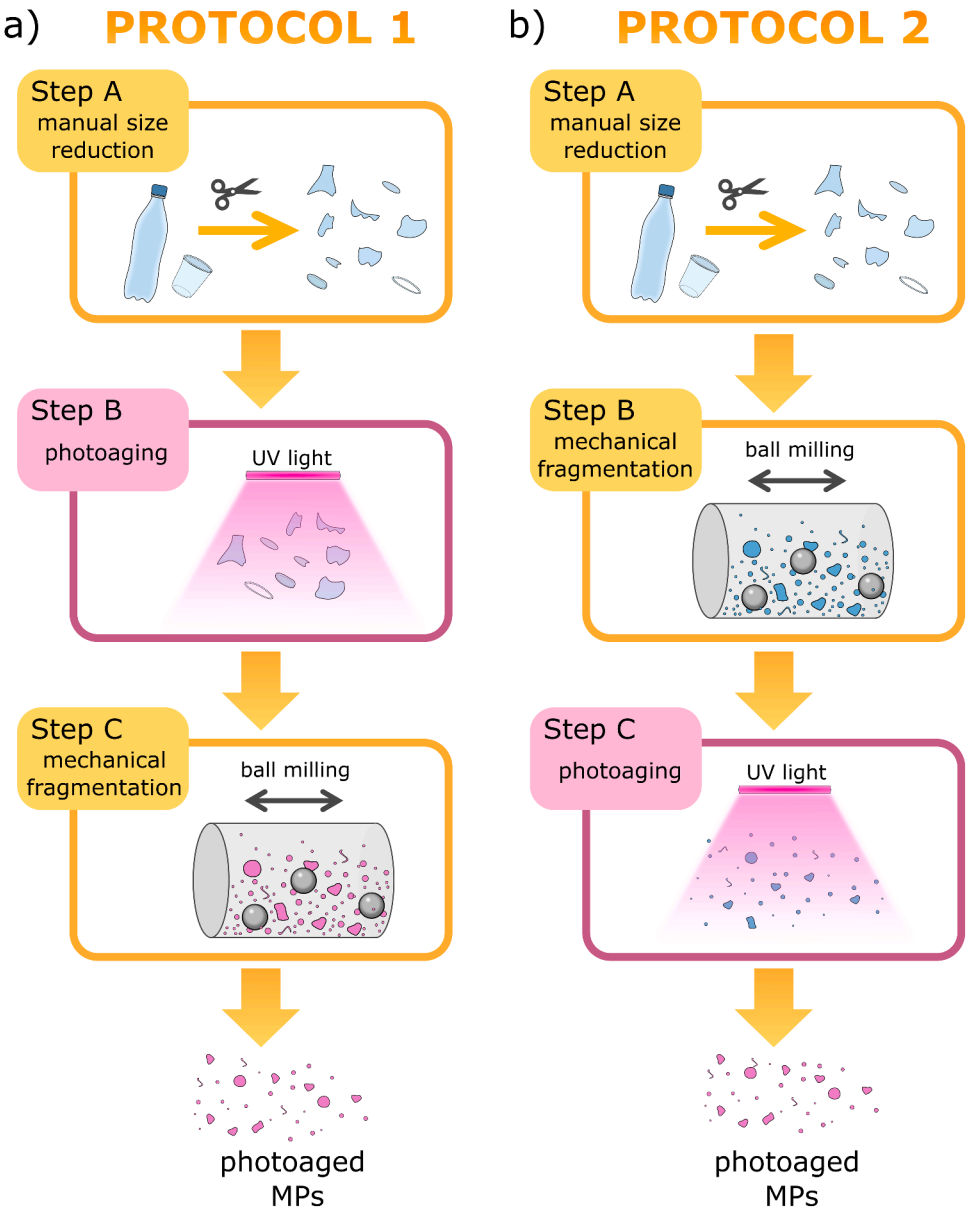

Fig. 1. Schematic representation of the (a) first aging protocol: macroplastic pieces from everyday products were UV-aged for up to eight weeks. Weekly, selected pieces per polymer were removed and fragmented through mechanical milling to produce MP powders. (b) Second aging protocol: macroplastic samples were fragmented using a mixer mill and then subjected to eight weeks of aging.

collected as blank controls prior to the aging process at 0 week. For the second approach, two independent MP productions were tested to enhance the robustness of the measurement results. In contrast, duplicates were not produced for the first protocol, as the results were too variable, with no clear trends or reliable data to support meaningful discussions or conclusions. Moreover, the preparation protocols were highly time-consuming and, particularly in the case of the first protocol, required considerable laboratory space and logistical effort. For this reason, an independent experimental replication was only performed for the protocol that proved more promising in terms of chemical homogeneity of the generated MPs, ensuring that resources were focused on the most reliable and environmentally relevant preparation method.

2.3. Artificial aging protocols

A UV furnace box system equipped with 4 × 30 W UVC bulbs (Philips TUV 30W/G30T8 lamps), with the main wavelength at 254 nm, operating in air and set at 42 °C with approximately 85 % relative humidity, was used to induce photo-oxidation. The UV light spectrum, characterized and presented in Figure S2 of the Supplemental Material, was measured using a fiber optic UV–Vis spectrometer (Ocean Optics, Orlando, FL, United States) and compared against the manufacturer technical data sheet. The irradiance within the UV box was mapped using a Spectral Light Meter (S120VC - Standard Photodiode Power Sensor, UV-Extended Si, 200 - 1100 nm, 50 nW - 50 mW, Thorlabs Inc. Newton, New Jersey, United States). The sensor was positioned at the bottom of the box, about 20 cm away from the lamps. Measurements were taken at nine locations across the box, with each location in triplicate, to cover the entire box surface. The mean irradiance at the bottom of the box resulted 41 W/m^2 (Standard Deviation, SD = 5 W/m^2), predominantly from UVC (≈40 W/m^2) with a minor contribution from UVA (≈1 W/m^2). In the first protocol, selected pieces of each plastic type were removed from the UV box every week for fragmentation, with the final samples having been exposed to UV radiation for a total of 8 weeks. In the second protocol, aliquots of approximately 150 mg of MPs were collected weekly over the 8-week artificial aging process. As a

comparison, the mean global horizontal irradiation in Italy is about 170 W/m^2 (4.07 kWh/m^2 per day (Global Solar Atlas 2025), of which approximately 6.5 % corresponds to UV radiation (around 11 W/m^2 (ISO 4892–1:2016 2020; Suga et al., 2020). Based on these values, the artificial aging exposure applied in this study (1–8 weeks) can be roughly equated to natural exposure periods ranging from about 25 to 200 days, corresponding to an acceleration factor of ~3.7. It should be noted, however, that this comparison refers only to the overall irradiance values in the UV range. In our setup, the irradiation was dominated by UVC (≈40 W/m^2), whereas under natural environmental conditions UV radiation is almost entirely restricted to UVA and UVB, since UVC is absorbed by the atmosphere. This spectral difference may lead to distinct degradation pathways: UVC photons carry higher energy and are therefore more efficient in breaking polymer bonds, often resulting in a faster formation of oxidation products and surface embrittlement. By contrast, UVA/UVB-induced aging in the environment tends to be slower and more progressive, usually involving surface photo-oxidation processes combined with weathering factors such as temperature fluctuations, moisture, or mechanical abrasion. For this reason, the equivalence provided here should be regarded only as a first-order estimation, highlighting the acceleration effect of the artificial protocol rather than a strict correspondence with natural aging.

2.4. Near infrared spectroscopy (NIR)

The Miniaturized MicroNIR OnSite-W spectrometer (Viavi, California, United States) was employed to acquire spectra in the near-infrared region. This instrument utilizes a Linear Variable Filter (LVF) as the dispersive element, which is directly coupled to a linear detector array consisting of 128 pixels of InGaAs photodiodes, operating within the wavelength range of 950–1650 nm. Illumination is provided by two integrated tungsten light bulbs. Spectra were acquired in diffuse reflectance mode at a nominal spectral resolution of 6.2 nm, with five replicates collected on random points for each sample on MP powder fragmented for the first protocol and directly in-site in the UV furnace for the second protocol. Reference and dark measurements were recorded approximately every 10 min, using a white reference standard and a sheet of aluminum. Each scan had an integration time of 12.6 ms, and the resulting spectrum was averaged over 100 scans.

In order to monitor the aging process, a Principal Component Analysis (PCA) was carried out on NIR spectra. For each polymer, the corresponding spectra were collected in a single matrix (samples x wavelength) and imported in MATLAB environment. Before multivariate modelling, spectra were processed using the Savitzky-Golay second-derivative with a seven-point window and a second-order polynomial, followed by Standard Normal Variate (SNV) correction, and column mean-centering. All calculations were executed in MATLAB 2023b (The MathWorks, Inc, Natick, MA, USA) by means of PLS-Toolbox (Eigenvector Research, Inc. Manson, Washington, USA).

2.5. Fourier-transform infrared microspectroscopy (FTIR)

FTIR analysis was performed on the MP particles after both aging protocols with a Nicolet iN10 Infrared Microscope (Thermo Scientific, Milano, Italy) in transmittance mode with Barium Fluoride (BaF_2) window. Each spectrum was collected with a spectral resolution of 8 cm^{-1} at 16 scans, with the collection of five repetitions per sample on all the materials in the form of MPs.

To evaluate chemical modification due to the photodegradation, the carbonyl area of all spectra was monitored. The CI was calculated as the ratio between the integrated absorbance band of the carbonyl (C=O) peak from 1850 to 1650 cm^{-1} and the absorbance area of the reference bond (W. Conradie et al., 2022).

$$CI = \frac{Area\ of\ absoption\ peak\ of\ carbonyl\ bond}{Area\ of\ absorption\ peak\ for\ reference\ bond}$$

For PS, PP, HDPE, and PVC, the reference peak is related to CH_2 scissoring (1400–1500 cm^{-1}) (Almond et al., 2020; M.N. Miranda et al., 2021; Yousif et al., 2012).

CI was calculated considering the average of the five repetitions, and the error of the calculation was considered as the standard error, i.e., the standard deviation of the distribution (Altman and Bland, 2005).

2.6. Scanning electron microscopy (SEM)

SEM analysis was performed on unaged MP particles (0 week) and on MP particles aged using the second photoaging protocol (i.e., aging after fragmentation, at week 8), which was selected because it provided particles with a more homogeneous degree of aging. A small amount of MP samples was deposited onto aluminum stubs covered by carbon adhesive disks and was sputter-coated with gold. SEM micrographs were acquired with a SEM Alpha (SEC.Co., South Korea) using a secondary electron detector and an acceleration voltage of 15 kV.

2.7. X-Ray Diffraction (XRD)

XRD patterns were collected by a D8 Discover Micro-Diffractometer (Bruker, Germany) equipped with LYNXEYE XE-T Detector and Cu Anode X-Ray Tube (CuKα = 0.15406 nm), operating at 40 kV and 40 mA. The samples in triplicate were placed on a silicon support to avoid external contributions and were analyzed at room temperature in a 2θ range of 10° ÷ 60° (Collimator diameter: 2 mm; Step Size: 0.01° 2θ; Scan Step Time: 0.5 s).

2.8. Thermogravimetric analysis (TGA)

TGA was used to evaluate the effect of the aging processes on the thermal stability of polymers. TGA measurements were carried out using a PerkinElmer Pyris 1 analyzer (PerkinElmer, Waltham, MA, USA). About 3 mg of each sample were placed in a platinum open pan and heated from 50 °C to 700 °C at a heating rate of 10 °C/min. High purity nitrogen was fluxed through the furnace at a flow rate of 20 mL/min.

2.9. Differential scanning calorimetry (DSC)

DSC measurements were performed by means of a TA-Q2000 differential scanning calorimeter (DSC, New Castle, DE, USA) equipped with an RCS-90 cooling unit (TA Instruments). About 3 mg of samples were sealed into a Tzero aluminum pan. Measurements were performed according to the following thermal program: preliminary equilibration at 25 °C; heating ramp from 25 °C to 300 °C at a heating rate of 10 °C/min; isothermal for 2 min at 300 °C, cooling from 300 °C to 25 °C at 10 °C/min; second heating run from 25 °C to 300 °C at 10 °C/min. High-purity nitrogen was fluxed at 10 mL/min during the measurements. The crystallinity (X_c) index of a wholly crystalline PET, $\Delta H_m^0 = 140$ J/g (Porter, 1980) was calculated using the following equation:

$$X_c = \frac{\Delta H_m}{\Delta H_m^0} \times 100$$

where ΔH_m represents the melting enthalpy of the analyzed sample and ΔH_m^0 is the melting enthalpy of a wholly crystalline PET (140 J/g) (Porter, 1980).

2.10. Statistical analysis

For NIR measurements, five spectra were acquired for each polymer sample for each week of aging. In total, 225 spectra were collected for the first protocol, and 450 spectra were collected for the second protocol (two independent MP preparations). A representative spectrum for each sample is shown in Fig. 2, while all spectra were included in PCA analysis. For FTIR measurements, five spectra were acquired for each

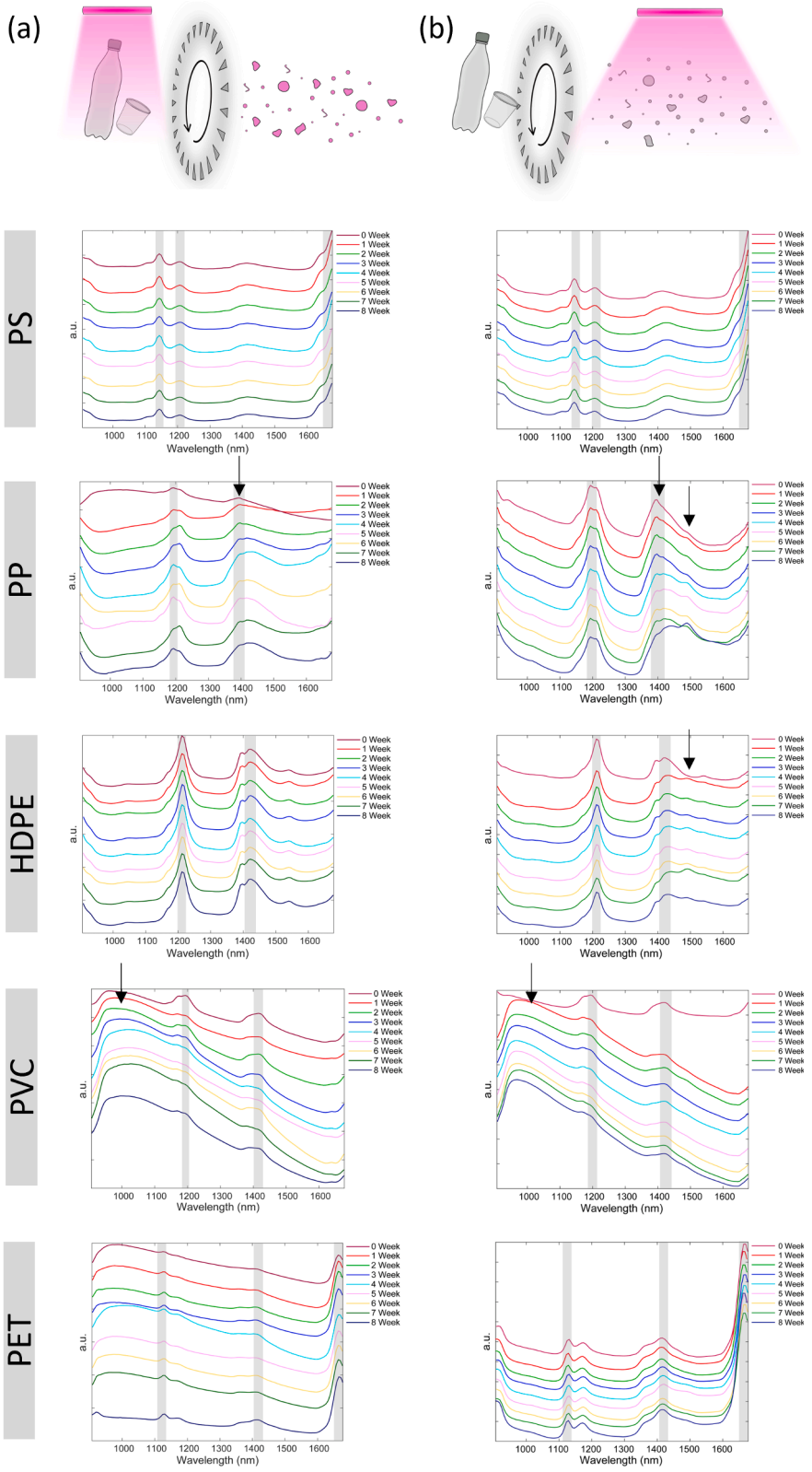

Fig. 2. Representative NIR spectra acquired on MP samples for all polymer types processed using: (a) the first protocol (aging followed by fragmentation); and (b) the second protocol (fragmentation followed by aging). au: arbitrary unit, the grey areas highlight the identifiable NIR bands, with changes induced by the photoaging indicated by arrows.

polymer sample for each week of aging. In total, 225 spectra were collected for the first protocol, and 450 spectra were collected for the second protocol (two independent MP preparations). A representative spectrum for each sample is shown in Fig. 4. For the calculation of CI, averaged spectral data for each sample were used. Duplicates were considered separately, and Student's *t*-test for paired data with a significance threshold of $p \leq 0.05$ was applied to compare the results.

3. Results and discussion

3.1. Material selection

The selection of the materials (PS, PP, HDPE, PVC, and PET) aimed to cover polymers most frequently reported in environmental samples, including both high- and low-density plastics with different crystallinity degrees (Petersen and Hubbart, 2021; Chang et al., 2022), and includes some of the priority polymers of regulatory interest, such as those listed in the Delegated Regulations under the Drinking Water Directive (ANNEX to the Commission Delegated Decision supplementing Directive (EU) 2025). These polymers were also previously characterized in detail in our earlier works on test material preparation via mechanical fragmentation protocols, which provided a solid basis for their inclusion in the present study (Ducoli et al., 2025). A maximum particle size of 500 μm was selected to generate MPs that are both environmentally relevant and representative of the size class most frequently reported in field surveys (Alfaro-Núñez et al., 2021; Lindeque et al., 2020). Moreover, particles within this sub-millimeter range undergo more homogeneous aging under UV exposure, as larger particles are prone to surface-only degradation, resulting in heterogeneous chemical and physical properties (Nagai et al., 2005; E. Kuka et al., 2024).

3.2. Artificial aging approach

The environmental weathering of plastics and the consequent formation of MPs is driven by a variety of degradation mechanisms, including mechanical abrasion, photodegradation, microbial colonization, and hydrolysis. The relative importance of these processes depends on multiple factors, such as the environmental matrix, geographical location, seasonality, and the polymer/additive composition. Because of this complexity, no single aging protocol can comprehensively reproduce real-world conditions. In this study we focused specifically on photodegradation, as it represents a major driver of polymer weathering in many environmental contexts. A univariate approach, where individual mechanisms are investigated separately, is a necessary first step to disentangle their specific contributions to the physicochemical and morphological properties of MPs. Nevertheless, it is important to acknowledge that in the environment these mechanisms often act simultaneously and synergistically. Future work will need to integrate multiple degradation pathways in order to capture such cooperative effects and generate test materials with the highest possible environmental relevance.

UV oxidation is an experimental method that accelerates the natural aging process of MPs, reducing the time required for aging and facilitating the production of aged test materials (Hüffer et al., 2018; Guan et al., 2022). UVC irradiation was selected to ensure the most efficient acceleration of the aging process, as it has been shown to significantly enhance the formation of aging-related chemical groups (Ouyang et al., 2022). In addition, UVC treatments are widely recognized for their efficiency in various applications (M.N. Miranda et al., 2021), such as microbial reduction in food (Ward et al., 2019) and in water and wastewater treatment, including hospital laundry wastewater (Zotesso et al., 2017). Consequently, MPs present in these environments, such as microfibers released during laundry (Napper and Thompson, 2016), can undergo aging processes due to exposure to UVC radiation. Furthermore, UVC radiation has been used in healthcare settings for disinfection, including in Heating, Ventilation, and Air Conditioning (HVAC) systems and operating room ceilings, with growing attention due to its effectiveness against multidrug-resistant bacteria and its relevance during the COVID-19 pandemic (Ethington et al., 2018; Lauritano et al., 2020). This study aims at proposing a robust protocol for generating environmentally relevant true-to-life MPs, by integrating controlled mechanical fragmentation with UV-induced degradation. The selected protocols to artificial weather plastic items followed a dual approach, simulating two distinct situations. The first one is intended to simulate the natural weathering of larger plastic items before they are broken down into smaller particles. Macroplastic items are firstly subjected to aging process and then mechanically fragmented. In the second one, plastic items are fragmented and sieved at 500 μm before the aging process occurring; this approach not only allowed us to directly study the effects of UV-induced aging on MP particles but also ensured that the MPs used in the experiments had consistent sizes and shapes, making them more suitable as uniform test materials for further research.

3.3. NIR spectroscopy

NIR spectroscopy is a non-destructive analytical technique used to identify materials based on their molecular vibrations, particularly in organic compounds like polymers. Portable NIR spectroscopy offers significant benefits for polymer analysis, as it allows for rapid, on-site identification and characterization of plastics without the need for extensive sample preparation, making it ideal for field applications and real-time decision-making. In NIR spectra, the bands typically correspond to overtone and combination modes of fundamental vibrations, mainly associated with C–H, O–H, and N–H groups. Their location is therefore characteristic of the polymer's chemical structure, while the relative intensity and shape of the bands provide information on compositional features and possible modifications during degradation. In this study, the portable microNIR spectrometer was exploited to track the aging effects on MPs, complementing FTIR measurement results.

Fig. 2 presents the NIR spectra acquired on MP samples for all polymer types across both protocols (first protocol in Fig. 2a, and second protocol in Fig. 2b). In general, the characteristic NIR bands were clearly identifiable for all selected plastic products (highlighted by the grey areas in Fig. 2). PS exhibited a dominant band around 1675 nm, along with smaller peaks near 1140 nm and 1205 nm. For PP and HDPE, two prominent bands were observed at approximately 1190 nm and 1400 nm for PP, and at 1210 nm and 1430 nm for HDPE. In the case of PVC, the primary peak was shifted outside the instrument's operating window, leaving only smaller peaks near 1190 nm and 1420 nm visible. The principal absorbance band for PET was located at 1660 nm, attributed to the first overtone of C–H stretching, along with smaller peaks around 1130 nm and 1415 nm (Rani et al., 2019).

3.3.1. First aging protocol

After the aging process following the first protocol, the specific effects of photoaging were variable across the polymers (Fig. 2a), with some showing notable photoinduced changes, while others remained stable in their NIR spectra throughout the weeks (changes are highlighted with arrows in Fig. 2). In the case of PS, no significant changes were detected, with only the characteristic peaks associated with the polymer appearing consistently over time. For PP, some slight modifications of the methyl and methylene (C–H) combination peaks at 1390 nm and 1400 nm started appearing from week 4, but with no clear distinctive indications of photoaging. The spectra for HDPE showed only the characteristic peaks with no significant changes due to aging. In contrast, PVC was the only polymer that started exhibiting notable features of photo-oxidation. In addition to the typical PVC peaks, a broad band around 1000 nm emerged in the aged samples (from week 1 to week 8), likely corresponding to the third overtone of the O—H group. Unlike the other polymers, where the first overtone was prominent, the third overtone of the O—H group appeared to play a more significant role in the oxidation process of PVC, suggesting a distinct mechanism

involving O—H species in PVC degradation. Finally, PET showed only its characteristic peaks throughout the aging process, with no visible signs of degradation or specific trends observed. By concluding, among the tested polymers, only PP and PVC exhibited some signatures of photoaging effects, while other polymers, including PS, HDPE, and PET, did not show prominent effects on the NIR spectra.

In order to further investigate subtle differences in the spectra, not ready visible by the spectral interpretation, some multivariate analyses

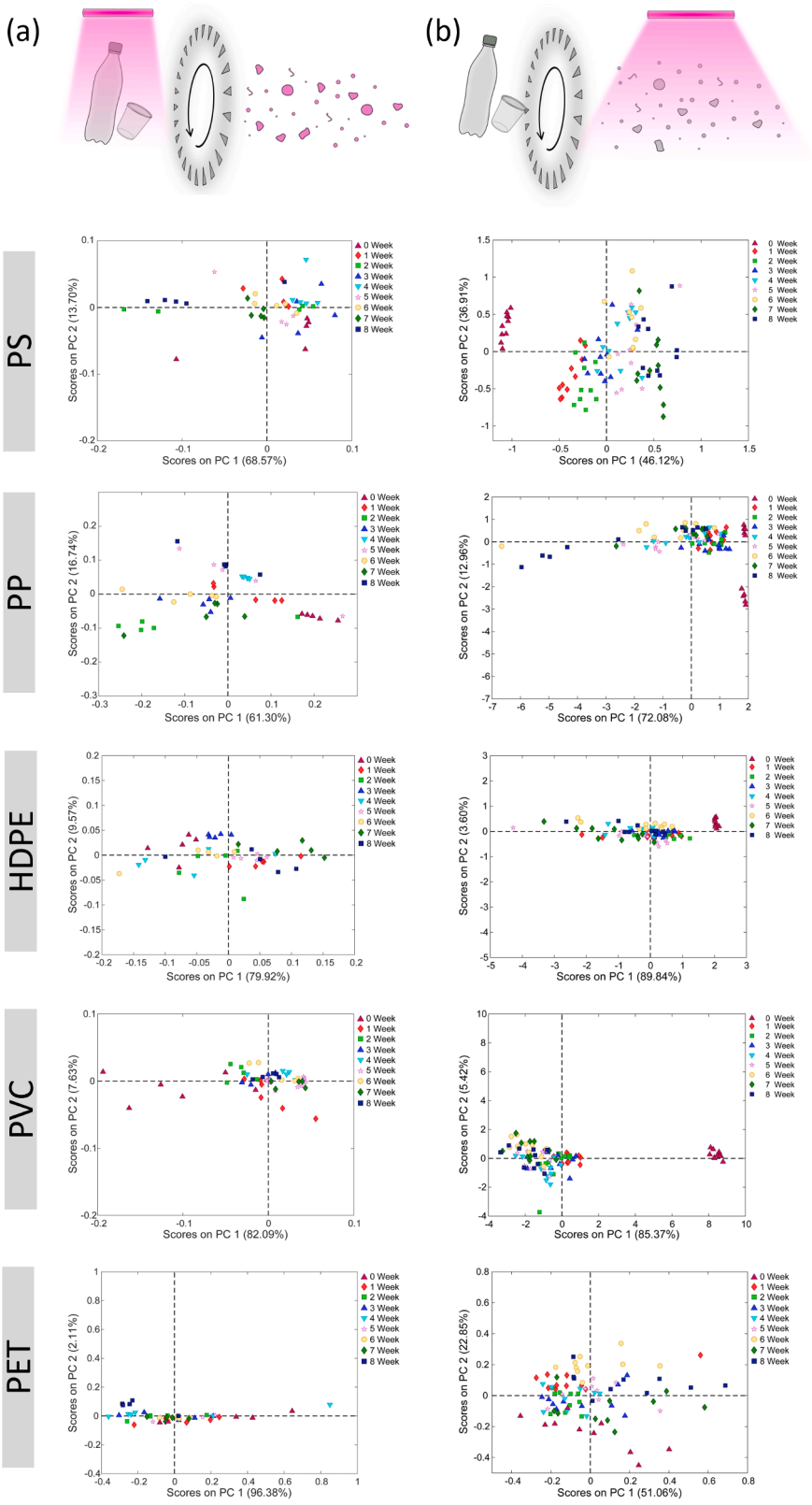

Fig. 3. PCA score plots based on NIR spectral data for MP samples for all polymer types processed using: (a) the first protocol (aging followed by fragmentation); and (b) the second protocol (fragmentation followed by aging).

were also applied to the spectra (Fig. 3). The PCA in Fig. 3a illustrates the unsupervised analysis of the entire dataset subjected to the first protocol of aging, showing the clustering of samples based on their aging status. Specifically, the PCA highlighted a slight grouping for PP and PVC, reflecting their possible susceptibility to photoaging, while the other polymers exhibited overlapping clusters, indicating minimal or no spectral differences post-aging. These findings provide some support for the hypothesis that photoaging effects in polymers are polymer-dependent, with certain materials (e.g., PP and PVC) appearing more prone to chemical and structural modifications. However, the evidence is not entirely conclusive, which could be attributed to the lack of homogeneity in the test materials. Indeed, only the surface of plastics was exposed to UV and after the fragmentation the inner virgin part was predominant. Subsequent fragmentation yielded pieces from both the surface and the interior, each exhibiting distinct and random chemical modifications. The surface fragments, which were more exposed to UV radiation, differed chemically from the internal fragments, which experienced less exposure. This suggests the need for a protocol that ensures more homogeneous test materials to further validate the hypothesis and clarify the underlying mechanisms driving these spectral changes.

3.3.2. *Second aging protocol*

After the aging process following the second protocol (Fig. 2b), we observed only the typical peaks in the NIR region associated with PS polymer, similar to the first protocol. However, in this case PCA revealed differences in the spectra due to the effects of aging. The PCA score plot, where samples are color-coded by aging time, is presented in Fig. 3b (first row). It is immediately evident that along PC1, the 0-week samples were completely differentiated from the other samples (1–8 weeks). Furthermore, for the aged samples (1–8 weeks), there was a noticeable increase in score values, ranging from −0.5 (1 week) to +0.75 (8 weeks). Thus, we can conclude that there was a clear distinction between the aged and non-aged samples, even though there were no significant visible spectral differences among the aged samples (1–8 weeks). To further validate these results, an analysis of the scores and loadings along PC1 can be conducted. However, this interpretation was avoided for PS due to the high complexity of its NIR spectra, particularly in attributing the NIR bands. In contrast, the analysis was completed for all the other polymers.

Focusing on PP, and specifically on the peaks related to methyl and methylene (C–H) combinations occurring at 1390 and 1400 nm, we observed that these peaks were present in samples aged 0 to 3 weeks. However, starting from the fourth week, degradation around these bands became noticeable. Specifically, from the fourth week onward, the peak around 1400 nm began to disappear, indicating a significant degradation process. Concurrently, a peak around 1490 nm, attributed to the formation of O—H species, became visible. The hydroxyl group was already present from the first week, but its prominence significantly increased starting from the fourth week, when the O—H peak became more evident. Moreover, during the last two weeks of aging, we observed a complete degradation of the methyl and methylene (C–H) combination band, with the disappearance of the two peaks and a strong presence of the O—H band. The PCA score plot for PP (Fig. 4b) showed a progressive movement of samples along PC1 as aging time increased, with this shift becoming more pronounced starting from the fourth week. Samples aged 0 to 3 weeks had positive score values (between 0 and 2), but starting from the fourth week, their scores turned negative, reaching highly negative values by the eighth week of aging. By analyzing the scores and loadings along PC1, as shown in Figure S3 in the Supplemental Material, we observed that the scores were linearly related to the aging time. In the corresponding loading plot, the second derivative of the peak related to the O—H group was correlated with the "week 0″ samples. It is important to note that this is the second derivative, meaning the peak was not present in the blank samples and only started to appear from the first week, becoming more prominent from the fourth week onward. Conversely, we can interpret the peak related to the methyl and methylene (C–H) combination band in the opposite manner; the second derivative of this peak was negative for the more aged samples, indicating that in the original spectra, the peak was no longer present.

For HDPE, in addition to the main peaks, we observed a broad band around 1490 nm starting from the first week. This peak is generally attributed to the first overtone of the hydroxyl group (Workman and Weyer, 2012). Therefore, the oxidation process started immediately, as the O—H group was detectable from the first week of aging. NIR spectroscopy is highly sensitive to the presence of O—H groups, making it advantageous for detecting early-stage oxidation in PE. These results were confirmed by PCA, as shown in Fig. 3b for HDPE. Along PC1 (which explained 89 % of the total variability), week 0 samples formed a tight, homogeneous cluster, clearly separated from the aged samples. The aged samples (1–8 weeks) were more scattered along PC1, with decreasing score values. To further confirm the occurrence of the oxidation process, we can examine the scores and loadings related to PC1 (Figure S3 in the Supplemental Material). We observed that the peak around 1490 nm had a positive contribution to PC1, contributing the most to the 0-week samples. It is important to note that we were analyzing the second derivative, so a strong positive derivative indicates that the peak was not present in the raw data and showed a downward concavity. Conversely, the peak began to appear starting from the first week, with a negative second derivative.

For PVC, in addition to the main peaks associated with the polymer, a broad band around 1000 nm became evident in the aged samples (1–8 weeks). This pronounced band was likely attributable to the third overtone of the O—H group (Pappa, 2010). In this case, a clear and immediate spectral change was observed, indicative of the photo-oxidation process. Unlike the other polymers, where the first overtone of the O—H group was more prominent, PVC exhibited a strong presence of the third overtone, likely reflecting a specific oxidation mechanism involving O—H species unique to PVC. The PCA score plot (PC1 vs. PC2) for PVC (Fig. 3b) shows that week 0 samples were completely differentiated from the aged samples along PC1. By examining the scores and loadings along PC1 (Figure S3 in the Supplemental Material), we can immediately note that the peak around 1000 nm was absent in the week 0 samples, as indicated by its positive second derivative, meaning the peak did not exist in the raw spectra. This strongly supports that the peak related to the third overtone of O—H was exclusively associated with the aged samples (1–8 weeks).

In the case of PET, only the typical peaks of PET were present, with no obvious signs of degradation. These findings are supported by the PCA results (Fig. 3b for PET), where the score plot (PC1 vs. PC2) showed that all samples were mixed together with no clear trend observed.

Except for the PET samples, the photoaging process following the second protocol affected the chemical composition of all particles in a more consistent and homogeneous manner, resulting in more reliable and comparable data compared to the first protocol. To further investigate the replicability of the process, we produced two independent sets of samples using the second protocol and assessed the uniformity of the results. To examine potential differences between the two replicates (designated as batch 1 and batch 2), we conducted a PCA analysis on the two sets. The score plot of the first two components is presented in Figure S4 in the Supplemental Material, with samples color-coded according to their respective batches. The two classes (batch 1 and batch 2) were connected by confidence ellipses at a 95 % level. Notably, there was complete overlap between the two categories for all five polymers, with the ellipses overlaying each other. Therefore, we conclude that there was no significant difference between batch 1 and batch 2.

These findings reinforce the reliability and consistency of the second protocol for studying the photoaging process across different polymer types. The observed uniformity in results between the two batches indicates that the methodology can be confidently replicated, supporting its application in future research on polymer degradation.

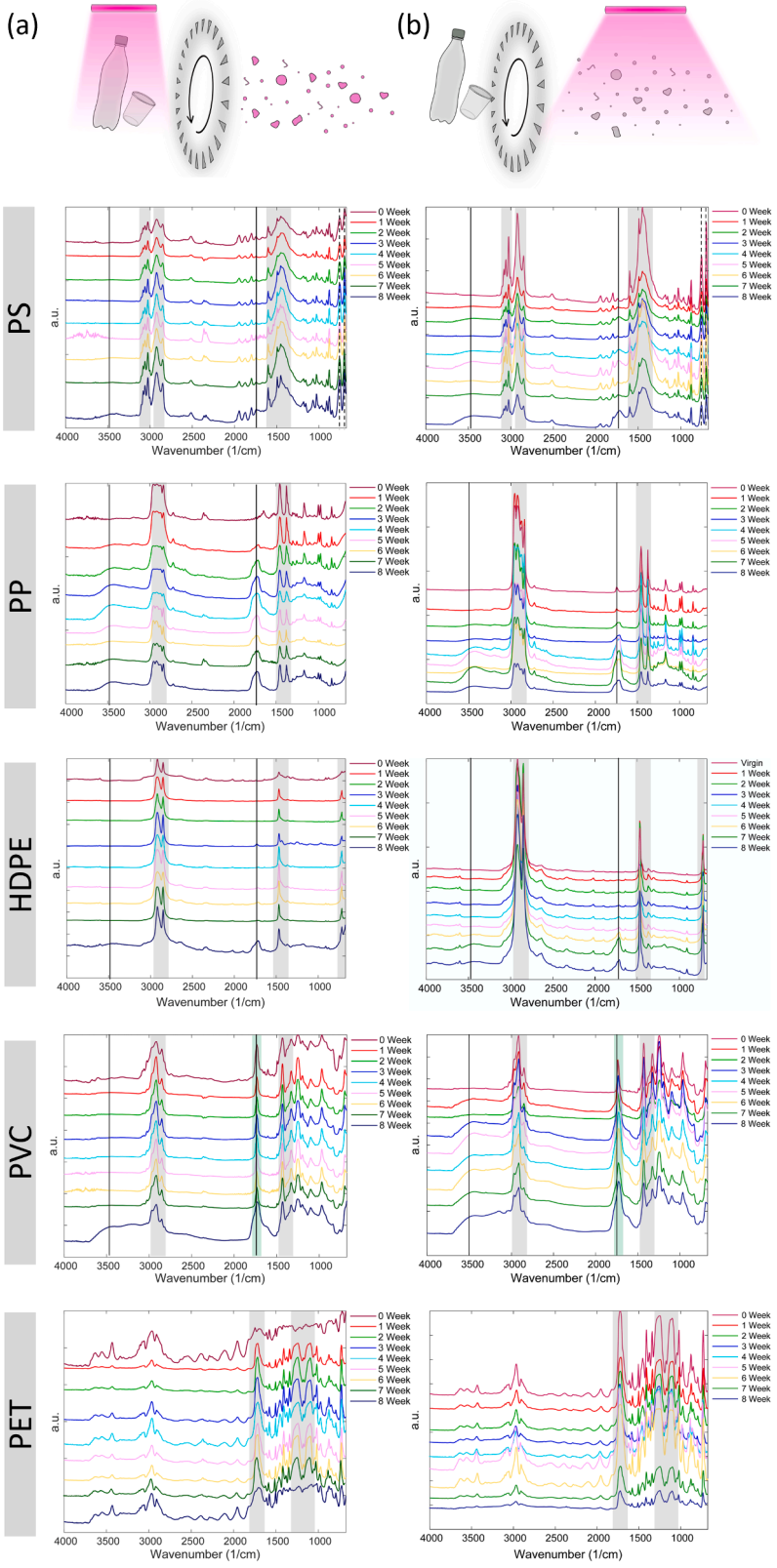

Fig. 4. Representative micro-FTIR spectra acquired on MP samples for all polymer types processed using: (a) the first protocol (aging followed by fragmentation); and (b) the second protocol (fragmentation followed by aging). The grey areas highlight the identifiable FTIR bands, the green area in PVC spectra highlights a possible contaminant in the plastic products. Vertical black solid lines indicate new functional groups after the photoaging process.

3.4. FTIR spectroscopy

FTIR spectroscopy is a powerful analytical tool extensively used for the identification of chemical bonds in various materials, including polymers, by measuring their infrared absorption spectra. For MP analysis, FTIR can be used in conjunction with microspectroscopy (micro-FTIR) to identify small particles in environmental samples, a method that has been extensively applied in research on environmental pollution. Additionally, FTIR is currently under investigation as part of the development of international standards for the identification and quantification of MPs, further solidifying its role as a key technique in environmental monitoring and regulatory frameworks (ISO/FDIS 16094–2 2020). In the context of photoaging of plastics, the CI is a key parameter used to monitor oxidative degradation processes. As plastics are exposed to UV radiation, photochemical reactions introduce carbonyl groups (C=O) into the polymer chains, which can be detected as an increase in absorbance at approximately 1700 cm^{-1} in the FTIR spectrum (E. Kuka et al., 2024; Strohriegl et al., 2021; W. Conradie et al., 2022). By calculating the CI, which compares the intensity of the carbonyl peak to a reference band that remains stable, researchers can quantitatively assess the extent of degradation, offering insights into the material's stability over time.

Fig. 4 shows representative FTIR spectra acquired on MP samples following both protocols (main bands highlighted by the grey areas in Fig. 4). Generally speaking, we can assign to PS samples the aromatic C—H stretching bond at about 3080, 3060 and 3025 cm^{-1}, while CH_2 symmetric and asymmetric stretching occurs at about 2920 and 2850 cm^{-1}, respectively (Smith, 2021). PS has the C—H stretches above and below 3000 cm^{-1}, because it contains saturated and unsaturated carbons. These latter come from the benzene ring, which have the so called "ring modes", derived from the stretching of the carbon-carbon bonds in the ring (Smith, 2021). These peaks occur from 1620 to 1400 cm^{-1}. PS has also the peak around 755 cm^{-1} which is related to the aromatic out-of-plane C—H bend, while at 695–700 cm^{-1} we can find a peak associated with the aromatic ring bend (Smith, 2021). IR spectra of PP samples show the main peaks ascribed to the asymmetric stretching of CH_3 bond which occurs at 2975–2950 cm^{-1}, while the CH_2 absorption occurs at about 2930 cm^{-1} (Krylova and Dukštiene, 2013). Regarding the symmetric stretching, we can observe the symmetric CH_3 vibration (Mazhar et al., 2014), which occurs at 2885–2865 cm^{-1} and the CH_2 vibration, which occurs at about 2870–2840 cm^{-1}. There is also the CH_3 asymmetric deformation vibration (Smith, 2021), which occurs at 1470–1440 cm^{-1}, and this band is overlapped with CH_2 scissor vibration (Gopanna et al., 2019), which occurs at 1490–1440 cm^{-1}. The most significant vibrational modes in HDPE are the C—H stretching around 3000 cm^{-1} and the -CH deformation modes around 1460 cm^{-1} and 1380 cm^{-1} (Wang et al., 2015; D'Amelia et al., 2016). We can also note the peak around 720 cm^{-1}, which is related to the rocking absorption of more than one methylene groups, - $(CH_2)_n$ (Rajeh et al., 2019). Regarding the PVC samples, the first consideration that applies to both sets of starting materials is the presence of the carbonyl group at around 1730 cm^{-1}, which can be attributed to the presence of vinyl acetate in the polymer mixture. Therefore, it is possible that the starting polymers were a copolymer of PVC and vinyl acetate, rather than pure PVC (green area highlighted in Fig. 4). Alongside this contaminant peak, we can note the presence of the peaks associated with C—H stretching at about 3000 cm^{-1}, and the peaks associated with CH_3 asymmetric deformation at 1470–1440 cm^{-1}. We can note also the CH_2 scissor vibration at 1490–1440 cm^{-1}, and the symmetric CH_3 vibration at 1390–1370 cm^{-1}. We can also note the presence of the band related to C—Cl stretching (Ul-Hamid et al., 2015) between 850 and 550 cm^{-1}. Furthermore, the C—O stretching (due to the acetate group) occurs at about 1228–1010 cm^{-1} (Acik et al., 2019). For PET, the characteristic IR absorption peaks can be observed at around 1720 cm^{-1} (C=O stretch) and near 1300 and 1100 cm^{-1}, corresponding to the C–O stretches of the C–C–O and O–C–C bonds, respectively. (Smith, 2018).

3.4.1. First aging protocol

After the aging process following the first protocol (Fig. 4a), some changes in functional group composition due to UV exposure appeared (indicated in Fig. 4 as black solid lines). For PS samples, the presence of O—H groups, indicated by the broad band around 3500 cm^{-1}, and a band at approximately 1720 cm^{-1}, related to the C=O group, were noticeable in the final week of aging. The presence of C=O and O—H groups can be associated with the photo-oxidation process (vertical black solid lines in Fig. 4). In PP samples, from the first week of aging, a broad band around 1850–1650 cm^{-1} could be observed, along with the band corresponding to the stretching of the O—H bond at around 3500 cm^{-1}. For HDPE samples, only a slight increase in the regions associated with aging processes (O—H bond and C=O group) was observed. In the case of PVC and PET, no significant differences in the FTIR spectra were noted.

3.4.2. Second aging protocol

After the aging process following the second protocol (Fig. 4b), the spectral analysis clearly demonstrated that all studied polymers, except for PET, underwent significant changes in functional group composition due to photo-oxidative aging. For PS samples, we could note that from the fourth week of aging, there was the presence of the O—H groups (broad band around 3500 cm^{-1}), and the presence of a band at about 1720 cm^{-1}, related to C=O group. The presence of the carbonyl group could be already observed also from the first week of aging. In case of PP samples, from the second week of aging, we could note the presence of a broad band around 1850–1650 cm^{-1}, and we could note that this band increased significantly starting from the fourth week of aging. Furthermore, there was also the presence of the band related to the stretching of O—H bond, which occured around 3500 cm^{-1}. Finally, we could identify a significant decrease in the height of peaks related to C—H bond, both for stretching bond and deformation bond; this was a further confirmation of the degradation process. Starting from the sixth week of HDPE samples, it was possible to identify an absorption peak in the range 1650–1850 cm^{-1}. This peak is related to the formation of carbonyl species (C=O), which occurred during the aging as a consequence of photo-oxidation. Furthermore, considering the last two weeks, it was possible also the identification of the broad band related to the stretching of O—H bond, which occured at 2500–3300 cm^{-1}. In the case of PVC samples, despite the presence of the interfering compound, we could note that the band of the C=O group was much wider in the aged samples with the presence of a very broad band. The aging was also confirmed by the presence of the band related to O—H bond at about 3500 cm^{-1}.

3.5. Carbonyl index

Fig. 5 presents a comparison of the calculated CI for the two different aging process across all polymers (except for PET samples). The results revealed a significant discrepancy between the two methodologies. In the first protocol, the aging of larger macro pieces resulted in a heterogeneous modification of both the exposed surface and the inner material. Subsequent fragmentation yielded pieces from both the surface and the interior, each exhibiting distinct and random chemical modifications. The surface fragments, which were more exposed to UV radiation, differ chemically from the internal fragments, which experienced less exposure. This variability was reflected in the CI analysis, where the values did not exhibit a consistent trend across all polymers. In light of this, the following discussion will focus exclusively on the second aging protocol. Specifically, the white dots in the plots of Fig. 5 represent the CI calculated as the average of the two independent batches, while Figure S5 in the Supplemental Material provides a comparison of the two independent batches. Generally, an increase in CI was observed from 0 to 8 weeks. While the individual batch comparisons are detailed in the Supplemental Material, overall agreement between batches was confirmed using a Student's *t*-test for paired data at each week. A significance threshold of $p \leq 0.05$ was applied to reject the null

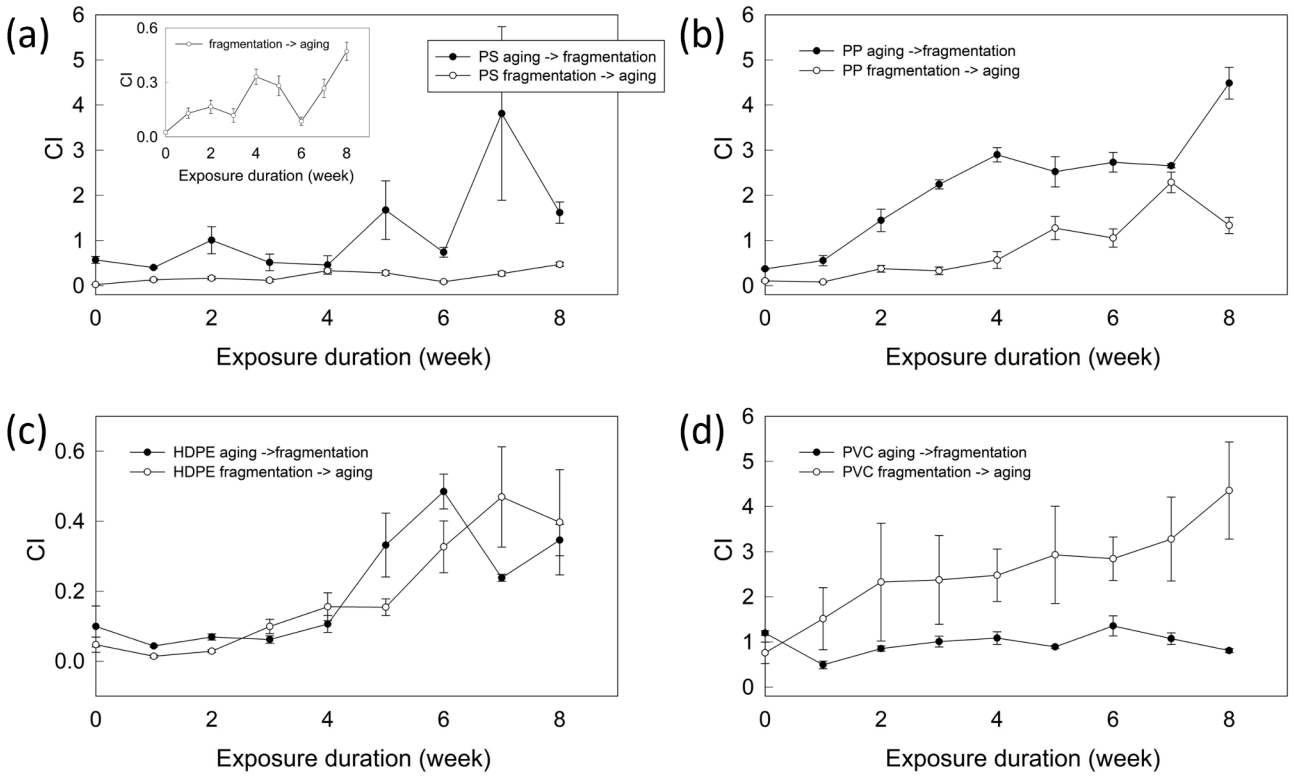

Fig. 5. Carbonyl Index calculated for (a) PS (with inset showing a zoom for the second protocol), (b) PP, (c) HDPE, (d) PVC MPs, processed using the first protocol (aging followed by fragmentation), and the second protocol (fragmentation followed by aging).

hypothesis (H_0). For all weeks, the null hypothesis was not rejected (p-value > 0.05), indicating no statistically significant differences between the batches. However, a few exceptions were noted, such as week 7 for PS and weeks 2 and 3 for PVC, as well as an unexpectedly lower value for week 6 for PS, likely due to experimental conditions or the chemical instability of the polymers during aging. A particular case is PP, where the CI increased steadily from 0 to 7 weeks before decreasing in the final week. This trend was consistent across both independent batches, as shown in Figure S5b in the Supplemental Material. In the first batch, CI ranged from (0.13 ± 0.04) to (2.32 ± 0.34) from weeks 0 to 7, with a decrease to (1.76 ± 0.23) in the last week, suggesting the onset of the so-called saturation behavior in the photo-oxidation process (Jiang et al., 2024; Toapanta et al., 2021). Batch 2 showed a similar trend, with CI ranging from (0.08 ± 0.02) to (0.91 ± 0.27), again confirmed by a Student's *t*-test. Similar trends of CI saturation/decrease for UV-aged PP MPs after a certain amount of exposure time was also observed in a recent paper [Das and Tiwari, 2019], even if the exact CI values are difficult to be compared due to the different experimental set-ups.

The differences observed between the two ageing protocols can be explained by the way UV radiation interacts with the polymer matrices. In the first protocol (UV exposure of macroplastic pieces before fragmentation), degradation occurred primarily at the surface, while the inner bulk remained largely unaffected. As a result, the subsequent fragmentation generated a heterogeneous mixture of particles, some strongly oxidized and others retaining their pristine chemical features. This explains the broader variability in CI values and the less distinct clustering observed in PCA analysis. In contrast, the second protocol (UV exposure after fragmentation) ensured that all particles, being smaller in size, were directly exposed to the radiation. This led to more uniform oxidative modifications across the polymer population, reflected in the consistent CI trends and the tighter clustering in PCA space. Building on this finding, and considering the more consistent and homogeneous chemical fingerprint obtained with the second protocol, we further investigated how photoaging affected the morphology of the resulting MPs. SEM imaging was therefore employed to evaluate size changes, fragmentation behavior, and surface modifications in MPs before and after aging, followed by TGA analysis to provide valuable insights into the thermal stability of the different polymers across the aging period, as described in the following sections.

3.6. Morphological analysis

Based on the more reliable chemical fingerprint obtained with the second protocol, additional characterizations were performed on this set of materials. In particular, SEM analysis was used to elucidate the impact of photoaging on particle morphology. Micrographs of the samples were taken at week 0 (unaged) and week 8 (UV-aged) at different magnifications to investigate both the size reduction of larger particles caused by secondary fragmentation induced by photoaging, as well as the shape and surface modifications of individual particles (Fig. 6).

Generally speaking, no severe changes in the morphology of the fragments was observed following aging. PS MPs showed a high tendency to aggregate when in the dry solid phase. Indeed, it is possible to note that bigger microparticles were covered by hundreds of tiny particles, reaching the nanometric range, instead of homogeneously distributing upon the deposition support. PS resulted in the plastic type most prone to fragmentation, among the five tested polymer types. The characteristic presence of small micro- and nanoparticles attached to the surface of bigger MPs was observed for both unaged and photoaged MPs, with no significant differences between the two treatments. PET and HDPE MPs, on the contrary, showed smooths particles surface and a flake-like morphology. Particles tended to be generally bigger compared to PS MPs, with few or no particles in the nanometric range. The main differences in MP morphology after photoaging were observed for PVC MPs, which showed a significant increase in the porosity of the fragments. While the MP surface of unaged PVC MPs appeared smooth, the surface of aged MPs revealed the formation of numerous porous. However, this particular feature was not homogenously observed for all MPs.

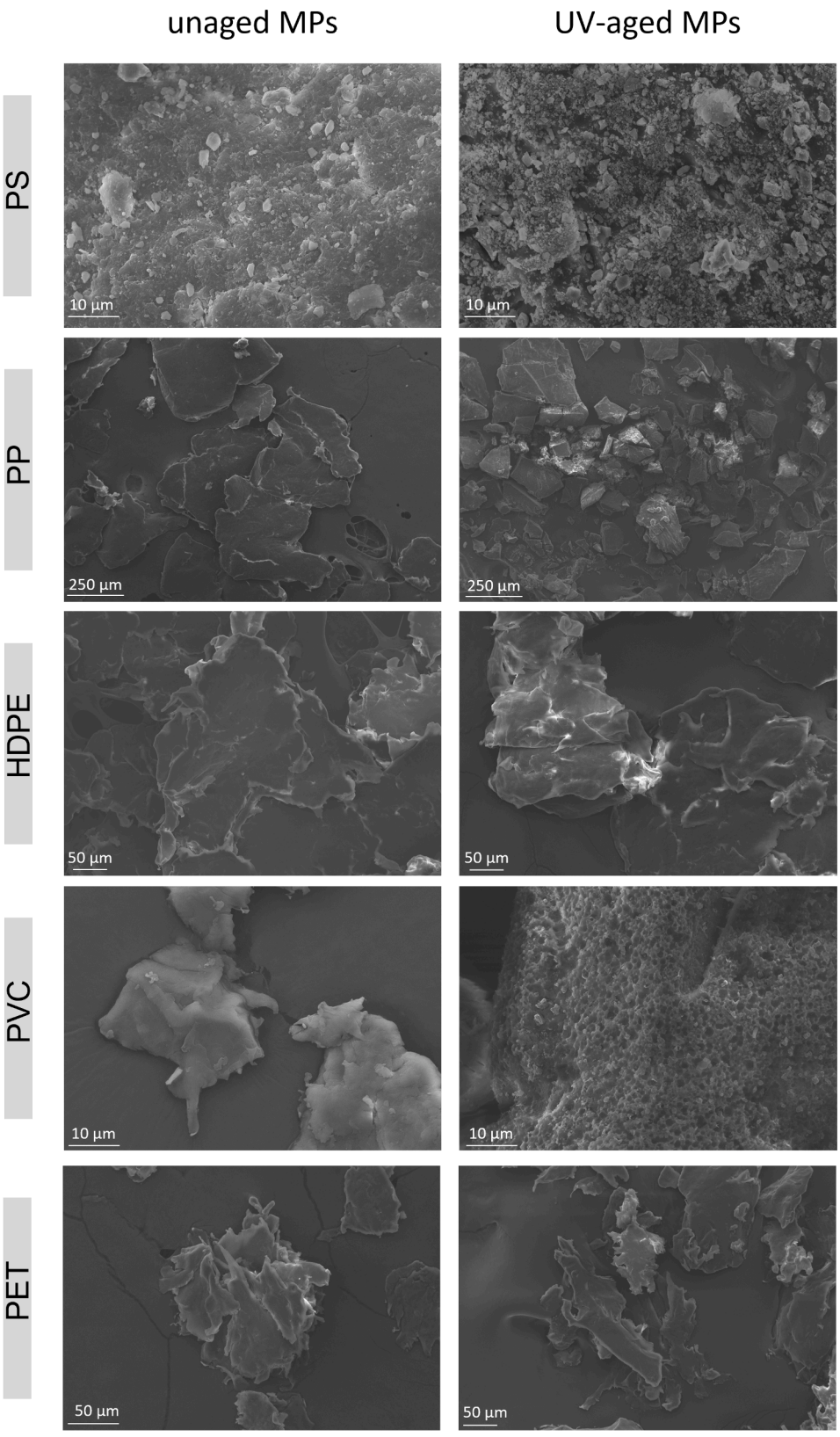

Fig. 6. SEM micrographs of unaged (0 week) and UV-aged (8 week) MPs for all polymer types processed using the second protocol (fragmentation followed by aging).

PP MPs also exhibited some alterations following the aging protocol, not in terms of single particle morphology, but rather in terms of particles size, suggesting that PP MPs suffered more from a secondary particle fragmentation induced by photoaging.

A possible explanation of the limited morphological changes observed for aged MP particles, despite the considerable chemical alterations revealed by NIR and FTIR analysis, is the mechanical fragmentation approach adopted for particle size reduction. Indeed, plastics were fragmented using a mixer mill, a quite impactful technique which was recently demonstrated to generate MPs with irregular morphologies and compromised crystallinity (Ducoli et al., 2025). Larger differences in the morphology of aged MPs compared to unaged counterparts could be better highlighted using a milder fragmentation approach, such as ultracentrifugal milling.

3.7. Thermogravimetric analysis

Plastic fragments aged following the second protocol were analyzed using TGA, to provide valuable insights into the thermal stability of the different polymers before and after aging period. In particular, unaged MPs and MPs aged for 8 weeks were analyzed, and the thermographs are reported in Fig. 7. The TGA curve of PS (Fig. 7a) shows a single major weight loss step, indicating that degradation primarily occured in one stage. PS typically degrades between 350 and 450 °C, with the primary breakdown occurring due to depolymerization into styrene monomers (Chigwada et al., 2008). PS MPs aged using the second protocol exhibited a slightly lower onset degradation temperature, suggesting a decrease in PS thermal stability due to aging.

PP (Fig. 7b) degraded with a single step. PP degradation occurs mainly via radical chain scission mechanisms, with decomposition typically starting between 350 and 450 °C (Mofokeng et al., 2012). The aged PP sample showed a slight shift to a lower onset temperature of degradation, indicating that some PP degradation occurred over the 8-week period.

HDPE (Fig. 7c) underwent a single major degradation step, associated with scission of C—C and C—H bonds (Al-Bayaty et al., 2020), that occured between 400 °C and 500 °C. Unaged and aged HDPE MPs presented a similar thermal stability, indicating that aging had a lesser impact on this material likely due to its highly crystalline structure, which offers greater resistance to degradation.

PVC degradation occured with a two-step process, with the first mass loss due to HCl evolution and the second corresponding to polyene decomposition, in the range of 200–500 °C (Wang et al., 2018). The aged sample showed minimal change in degradation behavior, indicating that slight oxidation effects might be present.

3.8. The case of PET

In the case of PET samples, using the CI as a quantitative measure for tracking the aging process is hindered by the strong presence of carbonyl groups in the unaged PET molecule, which already exhibit a characteristic and intense IR absorption peak around 1710 cm^{-1}, corresponding

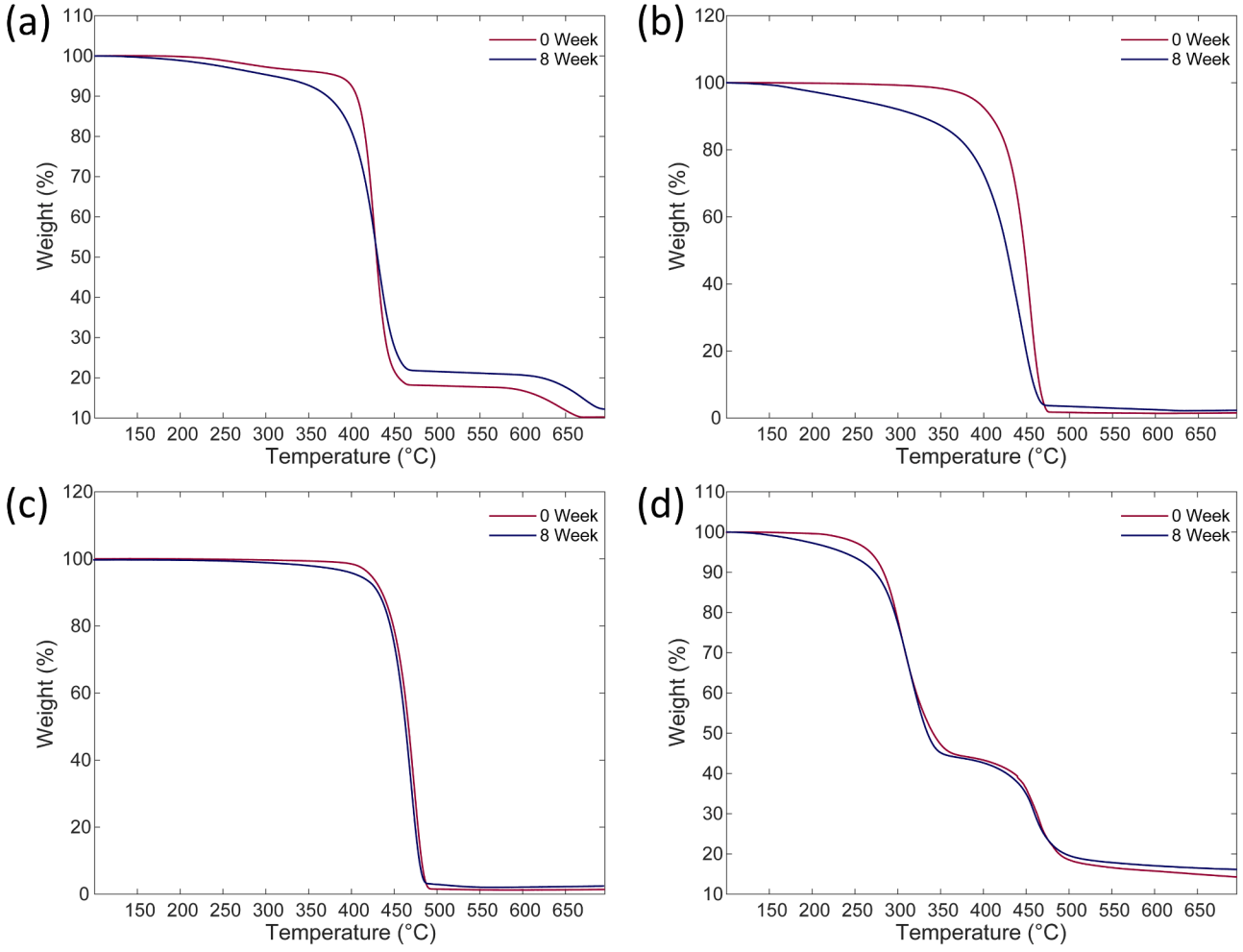

Fig. 7. TGA analysis of unaged (0 week) and UV-aged (8 week) MPs for all polymer types processed using the second protocol (fragmentation followed by aging). (a) PS, (b) PP, (c) HDPE, (d) PVC.

to the stretching of the C=O bond in the ester group (Tobin, 1957; Edge et al., 1996). No consensus has been reached in the literature regarding the calculation of CI for PET. Approaches range from simply avoiding the calculation of CI for PET (M.N. Miranda et al., 2021), to using the absorption band at 1720 cm^{-1} for the C=O group with a reference peak around 1400 cm^{-1} (W. Conradie et al., 2022), to employing the peak related to the C=C bond of the aromatic ring (1508 cm^{-1}) as the reference and the carbonyl peak at 1720 cm^{-1} (Pires et al., 2015). In the latter case, a decrease in CI during the aging process was observed. This approach was adopted in our study, but we did not detect any significant changes in the CI values. Figure S6 shows the CI for two independent batches, where the values remained almost constant, without the typical trend observed in other polymers. These results were confirmed using a Student's *t*-test, which demonstrated that, statistically, all values were equal, and no significant changes were detected. For this reason, we decided to complement spectroscopical analysis by XRD measurements for structural changes, and DSC and TGA investigations for thermal modifications.

Fig. 8 shows the XRD diffractograms for PET samples at extreme timing of aging, *i.e.*, week 0 before any UV exposure, and at the maximum exposure time in week 8. XRD was selected to assess potential structural changes, as any alterations in crystallinity or molecular ordering might indicate different aging behaviors not detectable via CI. The analysis revealed no significant changes in the diffractogram patterns, indicating that the polymer's structure remained stable throughout the aging process.

Further investigations included thermal analysis, in particular TGA to investigate thermal stability and degradation patterns, as variations in weight loss during heating can indicate the presence of aging-related chemical changes, and DSC to measure thermal transitions like melting or crystallization points, which can reveal how the polymer's thermal properties change due to aging. TGA and DSC measurement results are shown in Fig. 9a and 9b, respectively.

For the TGA, all curves exhibited a single major degradation step occurring between approximately 380 °C and 500 °C, which is characteristic of PET decomposition. This thermal degradation step is associated with the random scission of ester linkages that leads to the formation of oligomers and the release of volatile products (Das and Tiwari, 2019). Unaged and aged PET showed very similar degradation behavior, with almost no significant shifts in decomposition temperature.

The first heating run of the DSC thermogram is reported in Fig. 9, as it provides crucial insights into the material's thermal history related to the aging process and reveals properties that may be altered or lost in subsequent scans. For this reason, the glass transition temperature (T_g) and the melting temperature (T_m) have been detected from this run. The crystallization temperature (T_c), the onset crystallization temperature ($T_{c_{onset}}$), the melting temperature (T_m), the onset melting temperature ($T_{m_{onset}}$), and the degree of crystallinity (X_c) calculated from DSC thermographs are listed in Table 1. An endothermic peak appeared in all samples around 230–250 °C, corresponding to the melting of PET (Šudomová et al., 2023). Over the aging period, the shape and position of this peak remained unaltered, suggesting that the crystalline phase of PET did not undergo significant changes during PET aging.

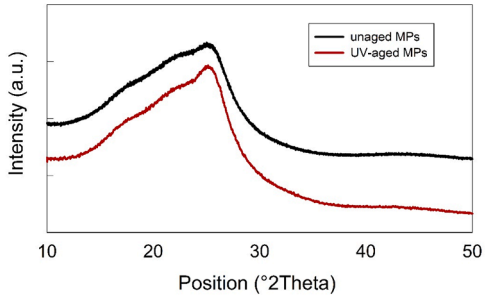

Fig. 8. Representative XRD diffractograms of unaged (0 week) and UV-aged PET MPs (8 week) processed using the second protocol (fragmentation followed by aging).

Both TGA and DSC analyses indicated no significant differences in PET thermal behavior or transitions, suggesting that the aging process did not induce any measurable changes.

The agreement in the obtained results with the behavior of the CI suggests that PET, under the tested conditions, is comparatively resistant to UV-induced degradation. However, this apparent inertness does not exclude the possibility of alternative degradation pathways, such as hydrolytic processes or chain scission events not detectable via CI or conventional thermal techniques. These findings underscore the importance of developing PET-specific aging markers and call for more advanced analytical approaches. Future investigations should explore non-carbonyl-based degradation mechanisms in PET, including hydrolysis and radical-driven depolymerization. The integration of high-resolution vibrational spectroscopy and modeling frameworks could offer a deeper understanding of degradation pathways, particularly for complex polymers like PET.

4. Conclusions

This study aimed to develop reproducible, environmentally relevant MP test materials through mechanical fragmentation and controlled UV-induced photoaging. By subjecting pre-fragmented MPs to eight weeks of UVC irradiation we observed general increases in the degree of aging across all polymers, with consistent trends between independent batches, demonstrating a reproducible route to prepare chemically homogeneous test materials. Although this protocol does not yet account for hydrolysis, biofilm formation, or other abiotic and biotic stresses, it nevertheless provides a robust and transferable starting point for ISO standardization and for the preparation of MPs for ecotoxicological, analytical, and remediation studies. The integration of NIR and FTIR spectroscopy, SEM, and TGA allowed for a multidimensional evaluation of MP aging. NIR and FTIR spectroscopy, combined with multivariate statistical analysis, facilitated the detection of subtle spectral changes and oxidation markers. CI analysis further confirmed progressive oxidation trends in the polymers, while SEM revealed some changes in surface morphology and fragmentation behavior. TGA added a thermal stability perspective, showing degradation-related shifts in onset temperatures for several polymers, thus reinforcing the chemical evidence of aging. Notably, the choice of analytical technique should consider polymer-specific sensitivities, as different polymers may exhibit distinct chemical, structural, and thermal responses during aging, highlighting the importance of combining multiple techniques to achieve a comprehensive and polymer-specific assessment of degradation processes.

Moreover, the approach developed in this study lays the groundwork for the adoption of true-to-life MP test materials, which are urgently needed to improve cross-study comparability and support regulatory and remediation strategies. Although the UVC source used in this study can be relevant for specific technological applications, such as the sterilization of medical plasticware and the disinfection of drinking water and wastewater, it is not representative of natural sunlight. Future developments may focus on different UV sources, as well as including other degradation pathways, like microbial colonization and hydrolysis, to increase the environmental relevance of final MPs. These materials featuring high environmental relevance can be further exploited to evaluate the environmental fate, toxicity, and biointeraction of MPs under realistic conditions, contributing to a more accurate risk assessment and the development of more effective mitigation solutions.

Funding information

This work was supported by the Italian Ministry of University and

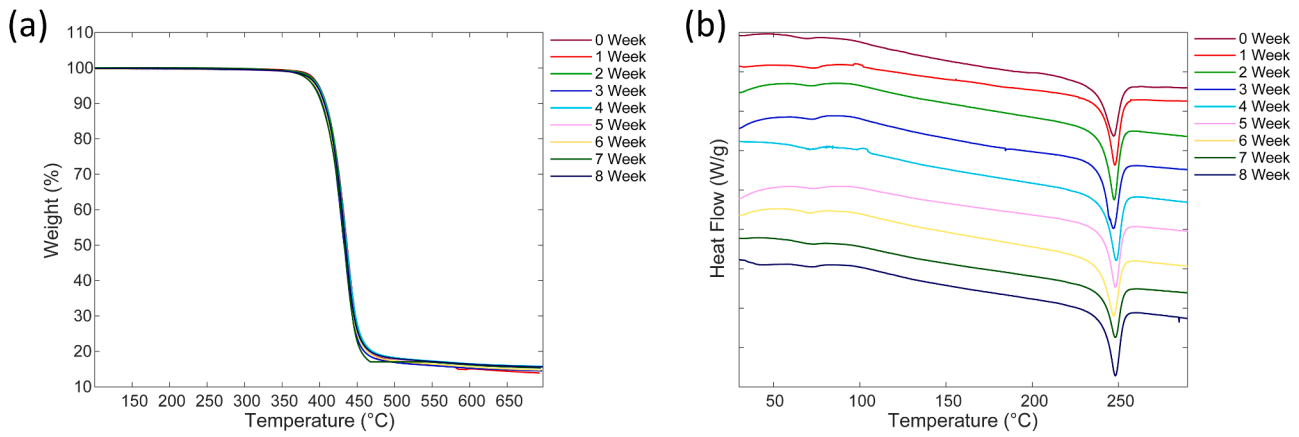

Fig. 9. PET MPs Thermal analysis: (a) TGA, (b) DSC.

Table 1
Thermal properties for PET.

	T_g (°C)	$T_{m\ ONSET}$ (°C)	T_m (°C)	$T_{C\ ONSET}$ (°C)	T_c (°C)	X_C (%)
VIRGIN	76.8	237.3	247.1	210.2	205.8	35.5
1 WEEK	78.2	241.5	247.9	205.2	197.6	39.6
2 WEEK	79.0	240.6	247.5	205.9	200.4	39.9
3 WEEK	75.9	240.2	246.8	205.2	197.8	38.6
4 WEEK	78.2	241.3	248.7	207.2	201.0	40.5
5 WEEK	83.4	241.5	248.2	206.3	200.0	42.0
6 WEEK	81.9	239.2	247.1	205.1	198.4	40.6
7 WEEK	72.9	240.9	248.0	207.0	201.1	43.5
8 WEEK	79.0	241.5	248.2	207.2	202.1	41.5

Research (Research program "Research Projects of National Relevance, PRIN 2022") and the project PLASTACTS 202293AX2L, CUP D53D23009050001.

CRediT authorship contribution statement

Serena Ducoli: Writing – original draft, Methodology, Investigation, Conceptualization. **Claudio Marchesi:** Writing – original draft, Methodology, Investigation, Conceptualization. **Mario Rigo:** Investigation. **Annalisa Zacco:** Investigation. **Erika Caianiello:** Investigation. **Rachele Castaldo:** Investigation. **Mariacristina Cocca:** Writing – review & editing, Methodology, Funding acquisition. **Stefania Federici:** Writing – review & editing, Writing – original draft, Methodology, Funding acquisition, Conceptualization. **Laura Eleonora Depero:** Writing – review & editing, Funding acquisition.

Declaration of competing interest

The authors declare that they have no known competing financial interests or personal relationships that could have appeared to influence the work reported in this paper.

Acknowledgements

This article is based upon work from COST Action CA20101 Plastics monitoring detectiOn RemedIaTion recovery—PRIORITY, supported by COST (European Cooperation in Science and Technology, www.cost.eu). S.F., R.C., and M.C. acknowledge the Italian Ministry of University and Research (Research program "Research Projects of National Relevance, PRIN 2022") and the project PLASTACTS 202293AX2L, CUP D53D23009050001.

Supplementary materials

Supplementary material associated with this article can be found, in the online version, at doi:10.1016/j.hazadv.2025.100905.

Data availability

Data will be made available on request.

References

Acik, G., Cansoy, C.E., Kamaci, M., 2019. Effect of flow rate on wetting and optical properties of electrospun poly(vinyl acetate) micro-fibers. Colloid Polym. Sci. 297, 77–83. https://doi.org/10.1007/S00396-018-4443-3.

Al-Bayaty, S.A., Al-Uqaily, R.A.H., Hameed, S., 2020. Study of thermal degradation kinetics of high density polyethlyene (HDPE) by using TGA technique. AIP Conf. Proc. 2290. https://doi.org/10.1063/5.0027503.

Alfaro-Núñez, A., Astorga, D., Cáceres-Farías, L., Bastidas, L., Soto Villegas, C., Macay, K., Christensen, J.H., 2021. Microplastic pollution in seawater and marine organisms across the Tropical Eastern Pacific and Galápagos. Sci. Rep. 11, 1–8. https://doi.org/10.1038/s41598-021-85939-3, 20211 11.

Almond, J., Sugumaar, P., Wenzel, M.N., Hill, G., Wallis, C., 2020. Determination of the carbonyl index of polyethylene and polypropylene using specified area under band methodology with ATR-FTIR spectroscopy. E-Polymers 20, 369–381. https://doi.org/10.1515/EPOLY-2020-0041.

Altman, D.G., Bland, J.M., 2005. Standard deviations and standard errors. BMJ 331, 903. https://doi.org/10.1136/BMJ.331.7521.903.

ANNEX to the Commission Delegated Decision supplementing Directive (EU) 2020/2184 of the European Parliament and of the Council by laying down a methodology to measure microplastics in water intended for human consumption https://environment.ec.europa.eu/publications/delegated-act-measure-microplastics-water_en. Accessed 12 Sep 2025.

Chang, X., Fang, Y., Wang, Y., Wang, F., Shang, L., Zhong, R., 2022. Microplastic pollution in soils, plants, and animals: a review of distributions, effects and potential mechanisms. Sci. Total Environ. 850, 157857. https://doi.org/10.1016/J.SCITOTENV.2022.157857.

Chigwada, G., Kandare, E., Wang, D., Majoni, S., Mlambo, D., Wilkie, C.A., Hossenlopp, J.M., 2008. Therma stabiliy and degradation kinetics of polystyrene/organically-modified montmorillonite nanocomposites. J. Nanosci. Nanotechnol. 8, 1927–1936. https://doi.org/10.1166/jnn.2008.027.

Conradie, W., Dorfling, C., Chimphango, A., Booth, A.M., Sørensen, L., Akdogan, G., 2022a. Investigating the physicochemical property changes of plastic packaging exposed to UV irradiation and different aqueous environments. Microplastics 1, 456–476. https://doi.org/10.3390/MICROPLASTICS1030033, 2022, Vol 1, Pages 456-476.

Conradie, W., Dorfling, C., Chimphango, A., Booth, A.M., Sørensen, L., Akdogan, G., 2022b. Investigating the physicochemical property changes of plastic packaging exposed to UV irradiation and different aqueous environments. Microplastics 1, 456–476. https://doi.org/10.3390/MICROPLASTICS1030033.

D'Amelia, R.P., Gentile, S., Nirode, W.F., Huang, L., 2016. Quantitative analysis of copolymers and blends of polyvinyl acetate (PVAc) using fourier transform infrared spectroscopy (FTIR) and elemental analysis (EA). World J. Chem. Educ 4 (2), 25–31.

Das, P., Tiwari, P., 2019. Thermal degradation study of waste polyethylene terephthalate (PET) under inert and oxidative environments. Thermochim. Acta 679. https://doi.org/10.1016/J.TCA.2019.178340.

De Boever, S., Devisscher, L., Vinken, M., 2024. Unraveling the micro- and nanoplastic predicament: a human-centric insight. Sci. Total Environ. 916, 170262. https://doi.org/10.1016/J.SCITOTENV.2024.170262.

Ducoli, S., Fambri, L., Gavazza, C., Bernatova, S., Abid, K., Spadaro, D., Foti, A., Donato, M.G., Gucciardi, P.G., Nalbone, L., Giarratana, F., Cocca, M., Castaldo, R., Federici, S., 2024a. Evaluating the effects of micro- and nanoplastics using true-to-life materials. In: 2024 IEEE International Workshop on Metrology for the Sea, MetroSea 2024 - Proceedings, pp. 334–337. https://doi.org/10.1109/METROSEA62823.2024.10765793.

Ducoli, S., Federici, S., Cocca, M., Gentile, G., Zendrini, A., Bergese, P., Depero, L.E., 2024b. Characterization of polyethylene terephthalate (PET) and polyamide (PA) true-to-life nanoplastics and their biological interactions. Environ. Pollut. 343. https://doi.org/10.1016/J.ENVPOL.2023.123150.

Ducoli, S., Rani, M., Marchesi, C., Speziani, M., Zacco, A., Gavazzi, G., Federici, S., Depero, L.E., 2025. Comparison of different fragmentation techniques for the production of true-to-life microplastics. Talanta 283. https://doi.org/10.1016/J.TALANTA.2024.127106.

Edge, M., Wiles, R., Allen, N.S., McDonald, W.A., Mortlock, S.V., 1996. Characterisation of the species responsible for yellowing in melt degraded aromatic polyesters - I: yellowing of poly(ethylene terephthalate). Polym. Degrad. Stab. 53, 141–151. https://doi.org/10.1016/0141-3910(96)00081-X.

Ethington, T., Newsome, S., Waugh, J., Lee, L.D., 2018. Cleaning the air with ultraviolet germicidal irradiation lessened contact infections in a long-term acute care hospital. Am. J. Infect. Control 46, 482–486. https://doi.org/10.1016/J.AJIC.2017.11.008.

Global Solar Atlas. https://globalsolaratlas.info/map. Accessed 12 Sep 2025.

Gopanna, A., Mandapati, R.N., Thomas, S.P., Rajan, K., Chavali, M., 2019. Fourier transform infrared spectroscopy (FTIR), raman spectroscopy and wide-angle X-ray scattering (WAXS) of polypropylene (PP)/cyclic olefin copolymer (COC) blends for qualitative and quantitative analysis. Polym. Bull. 76, 4259–4274. https://doi.org/10.1007/S00289-018-2599-0.

Guan, Y., Gong, J., Song, B., Li, J., Fang, S., Tang, S., Cao, W., Li, Y., Chen, Z., Ye, J., Cai, Z., 2022. The effect of UV exposure on conventional and degradable microplastics adsorption for Pb (II) in sediment. Chemosphere 286, 131777. https://doi.org/10.1016/J.CHEMOSPHERE.2021.131777.

Hernandez, L.M., Howarth-Forster, L., Sørensen, L., Booth, A.M., Vidal, A., Tufenkji, N., Sempéré, R., Schmidt, N., 2025. UV-degradation is a key driver of the fate and impacts of marine plastics. How can laboratory experiments be designed to effectively inform risk assessment? Mar. Pollut. Bull. 219, 118271. https://doi.org/10.1016/J.MARPOLBUL.2025.118271.

Hüffer, T., Weniger, A.K., Hofmann, T., 2018. Sorption of organic compounds by aged polystyrene microplastic particles. Environ. Pollut. 236, 218–225. https://doi.org/10.1016/J.ENVPOL.2018.01.022.

ISO 4892-1:2016, 2020. Plastics—Methods of Exposure to Laboratory Light Sources—Part 1: General Guidance. International Organization for Standardization, Geneva, Switzerland.

ISO/FDIS 16094-2, 2020. Water Quality — Analysis of Microplastic in Water — Part 2: Vibrational spectroscopy Methods For Waters With Low Content of Suspended Solids Including Drinking Water. International Organization for Standardization, Geneva, Switzerland. Under Publication.

ISO/TR 21960: 2020, 2020. Plastics—Environmental Aspects—State of Knowledge and Methodologies. International Organization for Standardization, Geneva, Switzerland.

Jiang, X., Gallager, S., Pàmies, R.P., Ruff, S.E., Liu, Z., 2024. Laboratory-simulated photoirradiation reveals strong resistance of primary macroplastics to weathering. Environ. Sci. Technol. 58, 14775–14785. https://doi.org/10.1021/ACS.EST.3C09891.

Krylova, V., Dukštiene, N., 2013. Synthesis and characterization of Ag layers formed on polypropylene. J. Chem. https://doi.org/10.1155/2013/987879.

Kuka, E., Cirule, D., Andersone, I., Vasiljevs, L.O., Merna, J., Sarakovskis, A., Kurnosova, N., Sansonetti, E., Vevere, L., Andersons, B., 2024a. A step to microplastic formation: microcracking and associated surface transformations of recycled LDPE, LLDPE, HDPE, and PP plastics exposed to UV radiation. Polym. Degrad. Stab. 229, 110967. https://doi.org/10.1016/J.POLYMDEGRADSTAB.2024.110967.

Kuka, E., Cirule, D., Andersone, I., Vasiljevs, L.O., Merna, J., Sarakovskis, A., Kurnosova, N., Sansonetti, E., Vevere, L., Andersons, B., 2024b. A step to microplastic formation: microcracking and associated surface transformations of recycled LDPE, LLDPE, HDPE, and PP plastics exposed to UV radiation. Polym Degrad Stab 229, 110967. https://doi.org/10.1016/J.POLYMDEGRADSTAB.2024.110967.

Kumari, S., Yadav, D., Yadav, S., Selvaraj, M., Sharma, G., Karnwal, A., Yadav, S., 2025a. From macro to micro: the key parameters influencing the degradation mechanism and the toxicity of microplastics in the environment. Polym. Degrad. Stab. 233, 111174. https://doi.org/10.1016/J.POLYMDEGRADSTAB.2025.111174.

Kumari, S., Yadav, D., Yadav, S., Selvaraj, M., Sharma, G., Karnwal, A., Yadav, S., 2025b. From macro to micro: the key parameters influencing the degradation mechanism and the toxicity of microplastics in the environment. Polym. Degrad. Stab. 233, 111174. https://doi.org/10.1016/J.POLYMDEGRADSTAB.2025.111174.

Lauritano, D., Moreo, G., Limongelli, L., Nardone, M., Carinci, F., 2020. Environmental disinfection strategies to prevent indirect transmission of SARS-CoV2 in healthcare settings. Appl. Sci. (Switz.) 10. https://doi.org/10.3390/APP10186291.

Lindeque, P.K., Cole, M., Coppock, R.L., Lewis, C.N., Miller, R.Z., Watts, A.J.R., Wilson-McNeal, A., Wright, S.L., Galloway, T.S., 2020. Are we underestimating microplastic abundance in the marine environment? A comparison of microplastic capture with nets of different mesh-size. Environ. Pollut. 265, 114721. https://doi.org/10.1016/J.ENVPOL.2020.114721.

Marchesi, C., Rani, M., Federici, S., Alessandri, I., Vassalini, I., Ducoli, S., Borgese, L., Zacco, A., Núñez-Delgado, A., Bontempi, E., Depero, L.E., 2023. Quantification of ternary microplastic mixtures through an ultra-compact near-infrared spectrometer coupled with chemometric tools. Environ. Res. 216, 114632. https://doi.org/10.1016/J.ENVRES.2022.114632.

Mazhar, M., Abdouss, M., Shariatinia, Z., Zargaran, M., 2014. Graft copolymerization of methacrylic acid monomers onto polypropylene fibers. Chem. Ind. Chem. Eng. Q. 20, 87–96. https://doi.org/10.2298/CICEQ120428104M.

Miranda, M.N., Sampaio, M.J., Tavares, P.B., Silva, A.M.T., Pereira, M.F.R., 2021a. Aging assessment of microplastics (LDPE, PET and uPVC) under urban environment stressors. Sci. Total Environ. 796. https://doi.org/10.1016/J.SCITOTENV.2021.148914.

Miranda, M.N., Sampaio, M.J., Tavares, P.B., Silva, A.M.T., Pereira, M.F.R., 2021b. Aging assessment of microplastics (LDPE, PET and uPVC) under urban environment stressors. Sci. Total Environ. 796, 148914. https://doi.org/10.1016/J.SCITOTENV.2021.148914.

Mofokeng, J.P., Luyt, A.S., Tábi, T., Kovács, J., 2012. Comparison of injection moulded, natural fibre-reinforced composites with PP and PLA as matrices. J. Thermoplast. Compos. Mater. 25, 927–948. https://doi.org/10.1177/0892705711423291.

Nagai, N., Matsunobe, T., Imai, T., 2005. Infrared analysis of depth profiles in UV-photochemical degradation of polymers. Polym. Degrad. Stab. 88, 224–233. https://doi.org/10.1016/J.POLYMDEGRADSTAB.2004.11.001.

Napper, I.E., Thompson, R.C., 2016. Release of synthetic microplastic plastic fibres from domestic washing machines: effects of fabric type and washing conditions. Mar. Pollut. Bull. 112, 39–45. https://doi.org/10.1016/J.MARPOLBUL.2016.09.025.

Ouyang, Z., Zhang, Z., Jing, Y., Bai, L., Zhao, M., Hao, X., Li, X., Guo, X., 2022. The photo-aging of polyvinyl chloride microplastics under different UV irradiations. Gondwana Res. 108, 72–80. https://doi.org/10.1016/J.GR.2021.07.010.

Pappa, H.N., 2010. Near-infrared spectroscopy. Pharmacopeial. Forum. 36, 532. https://doi.org/10.5772/24208.

Petersen, F., Hubbart, J.A., 2021. The occurrence and transport of microplastics: the state of the science. Sci. Total Environ. 758, 143936. https://doi.org/10.1016/J.SCITOTENV.2020.143936.

Pires, H.M., Mendes, L.C., Cestari, S.P., Pita, V.J.R.R., 2015. Effect of weathering and accelerated photoaging on pet/pc (80/20 wt/wt%) melt extruded blend. Mater. Res. 18, 763–768. https://doi.org/10.1590/1516-1439.010115.

Porter, R.S., 1980. Macromolecular physics, volume 3—Crystal melting, Bernhard Wunderlich, Academic Press, New York, 1980, 363 pp. Price: $42.50. J. Polym. Sci.: Polym. Lett. Ed. 18, 824. https://doi.org/10.1002/POL.1980.130181214. –824.

Rajeh, A., Morsi, M.A., Elashmawi, I.S., 2019. Enhancement of spectroscopic, thermal, electrical and morphological properties of polyethylene oxide/carboxymethyl cellulose blends: combined FT-IR/DFT. Vacuum 159, 430–440. https://doi.org/10.1016/J.VACUUM.2018.10.066.

Rani, M., Marchesi, C., Federici, S., Rovelli, G., Alessandri, I., Vassalini, I., Ducoli, S., Borgese, L., Zacco, A., Bilo, F., Bontempi, E., Depero, L.E., 2019. Miniaturized near-infrared (MicroNIR) spectrometer in plastic waste sorting. Mater. (Basel) 12, 2740. https://doi.org/10.3390/MA12172740, 2019, Vol 12, Page 2740.

Singh, S., S, S., Sachdev, S., Sahoo, K.S., Ambade, B., Bauddh, K., 2025. Microplastic pollution in agricultural environments: origins, impacts, and mitigation strategies. Phys. Chem. Earth 138. https://doi.org/10.1016/J.PCE.2025.103866.

Smith, B., 2018. Infrared spectral interpretation: a systematic approach. Infrared Spectr. Interpret.: Syst. Approach 1–304. https://doi.org/10.1201/9780203750841.

Smith, B.C., 2021. The infrared spectra of polymers III: hydrocarbon polymers. Spectrosc. (St. Monica) 36, 22–25. https://doi.org/10.56530/SPECTROSCOPY.MH7872Q7.

Song, Y.K., Hong, S.H., Eo, S., Shim, W.J., 2023. Fragmentation of nano- and microplastics from virgin- and additive-containing polypropylene by accelerated photooxidation. Environ. Pollut. 327, 121590. https://doi.org/10.1016/J.ENVPOL.2023.121590.

Sorasan, C., Edo, C., González-Pleiter, M., Fernández-Piñas, F., Leganés, F., Rodríguez, A., Rosal, R., 2022. Ageing and fragmentation of marine microplastics. Sci. Total Environ. 827, 154438. https://doi.org/10.1016/J.SCITOTENV.2022.154438.

Strohriegl, P., Senker, J., Meides, N., Menzel, T., Poetzschner, B., Löder, M.G.J., Mansfeld, U., Altstaedt, V., 2021. Reconstructing the environmental degradation of polystyrene by accelerated weathering. Environ. Sci. Technol. 55, 7930–7938. https://doi.org/10.1021/ACS.EST.0C07718.

Šudomová, L., Doležalová Weissmannová, H., Steinmetz, Z., Řezáčová, V., Kučerík, J., 2023. A differential scanning calorimetry (DSC) approach for assessing the quality of polyethylene terephthalate (PET) waste for physical recycling: a proof-of-concept study. J Therm Anal Calorim 148, 10843–10855. https://doi.org/10.1007/S10973-023-12430-8.

Suga, S., Blattner, P., Cordo, O., Cornell, G., Francis, A., Habte, A., Jung, J., Kita, H., Myers, D.R., Regan, J., Schönlein, A., Thorseth, A., 2020. Recommended Reference Solar Spectra for Industrial Applications. CIE - International Commission on Illumination. https://doi.org/10.25039/TR.241.2020.

Toapanta, T., Okoffo, E.D., Ede, S., O'Brien, S., Burrows, S.D., Ribeiro, F., Gallen, M., Colwell, J., Whittaker, A.K., Kaserzon, S., Thomas, K.V., 2021. Influence of surface oxidation on the quantification of polypropylene microplastics by pyrolysis gas chromatography mass spectrometry. Sci. Total Environ. 796, 148835. https://doi.org/10.1016/J.SCITOTENV.2021.148835.

Tobin, M.C., 1957. The infrared spectra of polymers. II. The infrared spectra of polyethylene terephthalate. J. Phys. Chem. 61, 1392–1400. https://doi.org/10.1021/J150556A030.

Ul-Hamid, A., Soufi, K.Y., Al-Hadhrami, L.M., Shemsi, A.M., 2015. Failure investigation of an underground low voltage XLPE insulated cable. Anti-Corros. Methods Mater. 62, 281–287. https://doi.org/10.1108/ACMM-02-2014-1352.

Wang, C., Wang, Y., Dang, Y., Jiao, Q., Li, H., Wu, Q., Zhao, Y., 2015. Synthesis of a novel titanium complex catalyst and its catalytic performance for olefin polymerization.

Russ. J. Appl. Chem. 88, 1723–1727. https://doi.org/10.1134/S1070427215100262.

Wang, K., Kou, Y., Wang, K., Guo, C., Liang, X., Wang, M., Li, J., Liang, S., Wang, W., Wang, J., 2025. Comparison of adsorption of seven ionic organic pollutants on polystyrene and poly(butylene adipate-co-terephthalate) microplastics: UV aging mechanism and role of charge-assisted hydrogen bond. Sep. Purif. Technol. 376, 134041. https://doi.org/10.1016/J.SEPPUR.2025.134041.

Wang, Z., Wei, R., Wang, X., He, J., Wang, J., 2018. Pyrolysis and combustion of polyvinyl chloride (PVC) sheath for new and aged cables via thermogravimetric analysis-fourier transform infrared (TG-FTIR) and calorimeter. Mater. (Basel) 11. https://doi.org/10.3390/MA11101997.

Ward, D.M., Patras, A., Kilonzo-Nthenge, A., Yannam, S.K., Pan, C., Xiao, H., Sasges, M., 2019. UV-C treatment on the safety of skim milk: effect on microbial inactivation and cytotoxicity evaluation. J. Food Process Eng. 42. https://doi.org/10.1111/JFPE.12944.

Workman Jr., J., Weyer, L., 2012. Practical guide and spectral atlas for interpretive near-infrared spectroscopy. Pract. Guide Spectr. Atlas Interpret. Near-Infrared Spectrosc. https://doi.org/10.1201/B11894.

Yousif, E., Salimon, J., Salih, N., 2012. New stabilizers for polystyrene based on 2-N-salicylidene-5-(substituted)-1,3,4-thiadiazole compounds. J. Saudi Chem. Soc. 16, 299–306. https://doi.org/10.1016/J.JSCS.2011.01.011.

Zhang, J., Hou, X., Zhang, K., Xiao, Q., Gardea-Torresdey, J.L., Zhou, X., Yan, B., 2025. Photochemistry of microplastics-derived dissolved organic matter: reactive species generation and organic pollutant degradation. Water Res. 269, 122802. https://doi.org/10.1016/J.WATRES.2024.122802.

Zotesso, J.P., Cossich, E.S., Janeiro, V., Tavares, C.R.G., 2017. Treatment of hospital laundry wastewater by UV/H2O2 process. Environ. Sci. Pollut. Res. 24, 6278–6287. https://doi.org/10.1007/S11356-016-6860-5.